Optimum Biodiesel Production from Palm Kernel Oil Using Heterogeneous Catalyst from Carbide Slag and Termite Hill Clay

Justina Oduwa Okhonmina*, Kessington Obahiagbon, Eghe Amenze Oyedoh

Department of Chemical Engineering, University of Benin, Nigeria

***Corresponding Author**

DOI: https://doi.org/10.51584/IJRIAS.2026.11030049

Received: 18 March 2026; Accepted: 24 March 2026; Published: 07 April 2026

ABSTRACT

This study is aimed at optimizing biodiesel production from palm kernel oil (PKO), using heterogeneous catalyst made from carbide slag and termite hill clay. The precursors (carbide slag and termite hill clay) were prepared and characterized. The composite catalyst was doped with $Zn(NO_3)_2$ by wet impregnation method. The PKO was characterized to obtain its different properties. Design of Experiments (DOE) was systematically used to study the effects of different variables on biodiesel yield and to ascertain the ideal conditions for optimum yield. The modelling was limited to RSM, using Box-Behnken design. The PKO's acid value, saponification value, average molecular weight, density, viscosity, moisture content, iodine value and peroxide value were obtained as 7.34 mgKOH/g oil, 234.18 mgKOH/g oil, 741.93 g/mol, 0.901 g/cm^3, 4.7 mPa.s, 1.09%, 18.7 mg I_2/100g oil and 16.2 mEq/kg respectively. The XRF results showed that the carbide slag contained 89.763% CaO, 4.036 % SiO_2, 3.880 % Al_2O_3, etc., while the THC contained 46.924% SiO_2, 24.144% Al_2O_3, 20.619 % Fe_2O_3, etc. The composite contained the required oxides for carrying out esterification and transesterification process simultaneously. The yield was observed to be significantly impacted by all the factors. RSM numerical optimization gave an optimum yield of 98.22% at 66.95 °C, 94.04 minutes, 11.98:1 alcohol/oil ratio, and 2.39 wt% catalyst loading. There was an overall reduction of 28.4% in yield between the first and sixth reactions, for the catalyst reusability studies, which catalysed six different reactions. The produced biodiesel was characterized and the properties were found to be in agreement with the ASTM D6571 and EN 14214 standards.

Keywords: Palm kernel oil, Carbide slag, Termite hill clay, Biodiesel, Response surface methodology

INTRODUCTION

The search for environmentally acceptable and sustainable alternatives for traditional fossil fuels is the foundation of research into biodiesel. One of the most crucial components of a nation's development has been recognized as sustainable energy, and the amount of this energy produced and used is considered to be a good indicator of that nation's degree of economic growth and development [4]; [58]; [69]. More energy sources are needed to meet life's basic needs as the world's population grows at an exponential rate [48]. The growing need for petroleum creates a challenge that necessitates looking for alternative [21].

Biodiesel is an alternate energy source which is made from biological components like vegetable or animal fats and used cooking oils. When compared to traditional diesel fuel, it is accepted to be a greener and more sustainable choice for a number of reasons [55]. Biodiesel is biodegradable, renewable, non-toxic and friendly to the environment [45]. Since biodiesel degrades more readily in the environment than conventional diesel fuel, it can have a less negative environmental effect in the event of spillages or leakages. Considering the fact that biodiesel comes from a variety of fuel sources, it can help provide energy security. It offers an alternative to diesel derived from petroleum, lowering reliance on fossil fuels and lowering the economic and geopolitical dangers connected with oil dependency [42].

Triglycerides, or fats and oils, are converted into biodiesel and glycerol by the process of catalysis, which is vital to the process. Both animal fats and different types of vegetable oils can be used to produce biodiesel [13].

ISSN No. 2454-6194 | DOI: 10.51584/IJRIAS |Volume XI Issue III March 2026

Transesterification is the most widely used technique for producing biodiesel [31]; [63]. It involves the reaction of triglycerides with alcohol (often methanol or ethanol) in the presence of a catalyst to produce glycerol and biodiesel [2]; [51]. Chemical reactions can be accelerated by catalysts without being used up in the process.

Homogeneous catalysts (alkali catalysts and acid catalysts), heterogeneous catalysts and enzymatic catalysts are the catalysts used in the production of biodiesel [33]. The two primary types of catalysts, which are mainly used are homogeneous catalysts and heterogeneous catalysts [51]. Alkali catalysts, such as potassium and sodium hydroxides, are frequently employed in their alkali hydroxide form [5]. In batch operations, they are useful in accelerating transesterification reaction [10]; [33]. Howbeit, they have certain disadvantages like the production of soap as a by-product and the requirement for further procedures to improve the produced biodiesel [19]. Transesterification can also be carried out using acid catalysts, such as hydrochloric or sulfuric acid [33]; [63]. However, because of the increased complexity of the reaction and the additional steps required to neutralize the acid and remove contaminants, acid-catalyzed transesterification is less prevalent [63]. Solid base catalysts, such as hydrotalcite or metal oxides, have drawn interest for the production of biodiesel [22]. They have the benefit of being easily separated from the reaction mixture, which eliminates the requirement for further purification processes [17]; [33]; [34]. Certain solid acid catalysts, such as zeolites or ion-exchange resins, have been studied for use in transesterification processes [46]; [65]. In comparison to homogeneous acid catalysts, they provide better selectivity and ease of separation [68]. By lowering the transesterification reaction's activation energy barrier and improving the reaction kinetics, catalysts enable the production of biodiesel under more favourable situations [36]. The feedstock being used, the intended reaction conditions, and the overall process economics all play a role in the catalyst selection [41]. Researchers persist in investigating and creating novel catalysts to enhance the effectiveness and sustainability of procedures involved in the production of biodiesel [3]; [33].

Response surface methodology (RSM) is a systematic approach, which aims to optimize the process and comprehend the correlations between different elements. Its main benefit is that it minimizes the number of experimental runs necessary to provide enough data for a result that is statistically significant [11]. RSM has been effectively used to investigate and optimize the production of biodiesel from a variety of feedstocks [57].

MATERIALS AND METHODS

Materials

The carbide waste and the termite hill clay used as precursors for the production of the heterogeneous catalyst were obtained from some welders' workshop and termite hills respectively, within Ugbowo environ in Benin City, Edo State, Nigeria. The palm kernel oil (PKO) used as the feedstock for the biodiesel production was obtained from a local vendor in Benin City, and its physiochemical properties are shown in Table 1.

Table 1: Physiochemical properties of PKO

Property	Value
Acid value (mgKOH/g oil)	7.34
Saponification value (mgKOH/g oil)	234.18
Average molecular weight (g/mol)	741.93
Density (g/cm^3)	0.901
Viscosity @ 40°C, 30.0 RPM & 22% (mPa.s)	4.7
Moisture content (%)	1.09
Iodine value (mg I_2/100g oil)	18.7
Peroxide value (mEq/kg)	16.2

Catalyst Preparation

The collected carbide slag sample was sun-dried and oven-dried at 110 °C until constant weight was achieved. The dried carbide slag was then pulverized and screened using a sieve of <200μm aperture to achieve a homogenous particle size. The prepared carbide slag was further processed by calcination at a temperature of 850 °C for 4 hrs in a Muffle furnace. In order to prepare the active phase support, the Termite Hill Clay (THC)

ISSN No. 2454-6194 | DOI: 10.51584/IJRIAS |Volume XI Issue III March 2026

was cleaned to get rid of impurities and then pulverized and screened with a sieve of <200 μm aperture. The clay was then oven dried at 110ºC for 12 hours to remove moisture. Calcination in a muffle furnace at 850ºC for 4 hours was done in line with the method prescribed by Olubunmi et al. [44], with little adjustment. The THC was then activated with 2M H_2SO_4. This was achieved by adding the acid to the clay in ratio 2:1, weight by weight, and stirred. The mixture was allowed to stay for 48hrs and thereafter washed and dried until the sample was completely dry. It was then calcined at 800ºC for 2 hrs 30 mins.

The composite material was synthesized according to the methods stated by Ajala et al. [1] and Olubunmi et al. [44], with slight modifications. Typically, a 200g of mixture of the prepared CARBIDE SLAG and THC was formulated in proportions of 20:80%, 40:60%, 50:50%, 60:40%, and 80:20% of CARBIDE SLAG to THC, giving 5 different samples. The samples were subsequently doped with equal amounts of 1.5M Zinc nitrate, in ratio 1:4 of the composite material to the zinc nitrate, using wet impregnation method to form suspensions, which were stirred for 6 hours on a magnetic stirrer at 80ºC for homogenization. The mixtures were allowed to stay and the excess liquid removed by decantation, while the slurries were placed in a vacuum oven to dehydrate at 120ºC until they were completely dry. The five different proportions of the doped dried composite material were pulverised and sieved with a sieve of <200 μm aperture. Each of the five different composite material was shared into 3 parts and calcined in a muffle furnace at 3 different temperatures, 650^0C, 750^0C and 850^0C, under static air conditions for 4 hours. The prepared catalysts were used to produce biodiesel to ascertain the one that will give the highest biodiesel yield. The catalysts that gave the highest three yields were again used for biodiesel production and the one that gave the highest yield was stored in an air-tight container for catalyst characterization and biodiesel production.

Catalyst characterization

The produced catalyst and individual precursors were characterized to evaluate their properties using Brunauer, Emmett and Teller (BET) analysis for surface area and pore properties determination, Fourier transform infrared (FTIR) spectroscopy analysis for bond structure and interaction, Scanning electron microscope (SEM) analysis for the surface structure, X-ray diffraction (XRD) analysis to show the crystalline phases, and X-ray Fluorescence (XRF) analysis to determine the chemical composition.

Biodiesel production

The transesterification process for the biodiesel production was a one-step procedure, based on the bi-functionality of the heterogeneous catalyst. A batch-type stirred reactor was used in the production process. 50g of the PKO was transferred into the reactor. The reactor comprised a 250ml conical flask, hot plate magnetic stirrer, a magnetic bar for stirring to ensure proper mixing for uniform mixture achievement, using a constant agitation speed. With the aid of the hot plate magnetic stirrer, the setup was heated to a specific temperature. Using the methanol to oil ratio and catalyst loading, methanol and catalyst mixture was added to the reactor for the transesterification reaction to occur for a set time [31].

The transesterification process was carried out based on the design matrix obtained from the design expert software. The reaction temperature, reaction time, methanol to oil ratio, and catalyst loading for each experimental run was given by the design matrix. The catalyst was separated from the biodiesel mixture after the reaction, with the aid of a centrifuge. It was then transferred into a separating funnel and allowed to stay overnight for proper settling. With the aid of the separating funnel, the glycerol in the bottom layer was run out. The biodiesel and the unreacted methanol left in the separating funnel were washed and transferred into a beaker and heated in an oven. The methanol evaporated, while the biodiesel was properly stored for characterization. The yield of biodiesel produced was determined using equation 1.

$$\text{Biodiesel yield} = \frac{\text{mass of biodiesel produced}}{\text{mass of PKO used}} \times 100 \quad (1)$$

ISSN No. 2454-6194 | DOI: 10.51584/IJRIAS |Volume XI Issue III March 2026

Fig 1: Biodiesel production process

Experimental design and Response surface methodology (RSM) modeling

Box Behnken Design (BBD) was used to design the transesterification process by systematically varying the input variables (reaction temperature, reaction time, methanol/oil ratio and catalyst loading) and the biodiesel yield was investigated. The ranges of the process variables are shown in Table 2.

Table 2: Process variables and their lower, middle and upper limits

Factor	Process variable	Units	Lower	Middle	Upper
A	Reaction temperature	°C	60	65	70
B	Reaction time	min	60	90	120
C	Methanol/oil ratio	mol/mol	6	9	12
D	Catalyst loading	(%wt)	1	3.5	6

The range of the input variables was determined from previous studies, with some modifications. The transesterification trials were a total of 29 runs. The factors were systematically varied at different levels. The response variable (biodiesel yield) was recorded. A quadratic regression model, as shown in equation 2, was fitted to the experimental data so as to model the transesterification process as a function of the input variables.

$$Y_i = b_o + \sum b_i X_i + \sum b_{ij} X_i X_j + \sum b_{ii} X_i^2 + e_i \quad (2)$$

Where, Y_i denotes the predicted response, b_o is the value at intercept, b_i is the coefficient of first order, b_{ii} is the quadratic effect coefficient, b_{ij} is the interacting effect coefficient, X_i and X_j are the process variables that affect the response, and e_i is the experimental random error [4].

RESULTS AND DISCUSSIONS

Catalyst characterization

X-ray Fluorescence (XRF) Analysis

Using XRF, the chemical composition of the precursors and produced catalyst (before and after use) were analysed. Table 3 shows the results of the analysis, which give useful perception of the oxides the precursors and produced catalyst comprise, thereby offering important information about their composition and potential catalytic activity. The carbide slag precursor's strong basicity and suitability as the primary source of basic active sites for transesterification reactions were confirmed by the XRF analysis, which revealed that it was primarily CaO-rich [1]. The THC precursor, on the other hand, had a much lower CaO content but larger SiO_2, AlO_3 and FeO_3 proportions, suggesting an aluminosilicate and iron structure that primarily supports structural stability and moderate acidity [26].

ISSN No. 2454-6194 | DOI: 10.51584/IJRIAS |Volume XI Issue III March 2026

The THC precursor diluted the CaO content during the formation of the composite catalyst, but it was still high enough to retain strong basicity. Both precursors were successfully integrated, as indicated by the intermediate quantities of SiO_2 and $Al2O_3$. Effective doping with zinc nitrate and its conversion to ZnO following calcination were amply demonstrated by the composite catalyst's notable rise in ZnO. Lewis acidic sites are introduced by this ZnO phase, which increases the esterification activity and allows the catalyst to operate bifunctionally for simultaneous esterification and transesterification [29].

Minimal changes in elemental composition are seen following catalytic application, with a relative rise in ZnO due to the loss of volatile or organic species and a slight decrease in CaO due to partial leaching or carbonation during reaction. The slight rise in SO_3 could be the result of adsorption or migration of sulfur-containing species, whereas small fluctuations in other metal oxides indicate surface remodeling and involvement in catalytic activities. On the whole, the XRF results show that the catalyst has good structural stability and validate the complementing functions of THC and carbide slag in producing a long-lasting and efficient bifunctional catalyst for the production of biodiesel.

Table 3: Elemental composition of carbide slag precursor, THC precursor, composite catalyst before use, and composite catalyst after use.

Component	carbide slag precursor	THC precursor	Concentration (%) of composite catalyst before use	Concentration (%) of composite catalyst after use
CaO	89.763	1.463	52.1448	49.853
SiO_2	4.036	46.924	10.3888	7.931
Al_2O_3	3.880	24.144	7.4389	7.9001
SO_3	0.583	0.388	0.2958	0.4005
Fe_2O_3	0. 439	20.619	5.2058	2.5286
Cl	0. 431	0.702	0.9034	0.7813
SnO_2	0. 246	0.000	0.2900	0.3453
TiO_2	0.131	3.804	0.9012	0.5234
CoO	0.088	0.090	0.0177	0.0108
BaO	0.085	0.000	0.0200	0.0211
SrO	0.061	0.026	0.0584	0.0346
CuO	0.055	0.145	0.0536	0.0387
Ta_2O_5	0.046	0.060	0.2323	0.2148
ZrO_2	0.028	0.513	0.2658	0.0978
Cr_2O_3	0.027	0.081	0.0340	0.0458
WO_3	0.024	0.000	0.5220	0.4491
NiO	0.023	0.005	0.0000	0.0000
PbO	0.014	0.035	0.0281	0.0333
V_2O_5	0.013	0.186	0.0746	0.0436
MnO	0.010	0.111	0.0388	0.0096
Cs_2O	0.008	0.090	0.0811	0.0365
ZnO	0.007	0.040	20.8653	23.0555
Rb_2O	0.002	0.010	0.0067	0.0183
Nb_2O_5	0.000	0.037	0.0331	0.0061
P_2O_5	0.000	0.182	0.0175	0.0026
MgO	0.000	0.000	0.000	5.5968
K_2O	0.000	0.308	0.0331	0.0006
Ag_2O	0.000	0.037	0.0492	0.0212

ISSN No. 2454-6194 | DOI: 10.51584/IJRIAS |Volume XI Issue III March 2026

X-ray diffraction (XRD) analysis

The XRD analysis was used to identify the crystalline phases and to determine the structure and physical properties of the calcine precursors and composite catalyst before and after use. Diffraction peaks typical of calcium oxide-derived phases are visible in the XRD pattern of the calcined carbide slag, with dominant reflections linked to calcium silicate and calcium-containing mixed oxides created during high temperature calcination, as shown in figure 2. The efficient breakdown of $Ca(OH)_2$ during calcination is confirmed by the absence or weak intensity of calcium hydroxide peaks [47]. Small reflections ascribed to calcium carbonate point to partial surface carbonation brought on by air exposure following calcination [55]. Broad diffraction peaks are advantageous for catalytic activity because they show partial amorphous character and small crystallite size. This implies that Calcined CARBIDE SLAG yields Ca-based basic phases that are thermally stable and appropriate for transesterification processes.

A highly crystalline aluminosilicate structure is indicated by the calcined termite hill clay's (THC) XRD pattern in figure 3, which shows distinct and sharp diffraction peaks. Quartz (SiO_2) and aluminosilicate phases, including mullite, which are produced or stabilized during calcination are shown by dominant reflections. With no collapse of the clay structure following heat treatment, the preservation of these peaks attests to the thermal stability of THC. This implies that during catalytic operation, calcined THC functions as a strong SiO_2–AlO_3 support that can disperse Ca-based active species and prevent sintering [71].

In figure 4 and figure 5, the XRD patterns for both the composite catalyst before and after use reveal diffraction peaks primarily located in the low-angle area between 10° and 30° (2θ), featuring a significant broad peak around 20–23°. This region is indicative of amorphous to poorly crystalline aluminosilicate and calcium silicate phases, demonstrating a strong interaction between CaO derived from carbide slag and the SiO_2–Al_2O_3 framework of termite hill clay. The minor diffraction peaks detected in the 25–35° (2θ) range are associated with crystalline SiO_2 (quartz) and calcium-containing mixed oxide phases, while the lack of sharp CaO reflections at higher angles (approximately 32°, 37°, and 54°) implies that free CaO has largely transformed into stable Ca–Al–Si mixed oxides.[18]; [27].

Following the production of biodiesel, phase rearrangement and partial carbonation during catalytic use caused the diffraction peaks to become slightly sharper and more intense, especially in the 20 – 30° (2θ) region [12]. This indicates an increase in crystallinity. Nevertheless, at higher diffraction angles, no new high-intensity peaks emerged, indicating that the composite catalyst maintained its structural stability after its use.

The shift from a poorly crystalline mixed oxide structure to a more crystalline phase that includes carbonate accounts for the minor deactivation of the catalyst following biodiesel production [25]; [52].

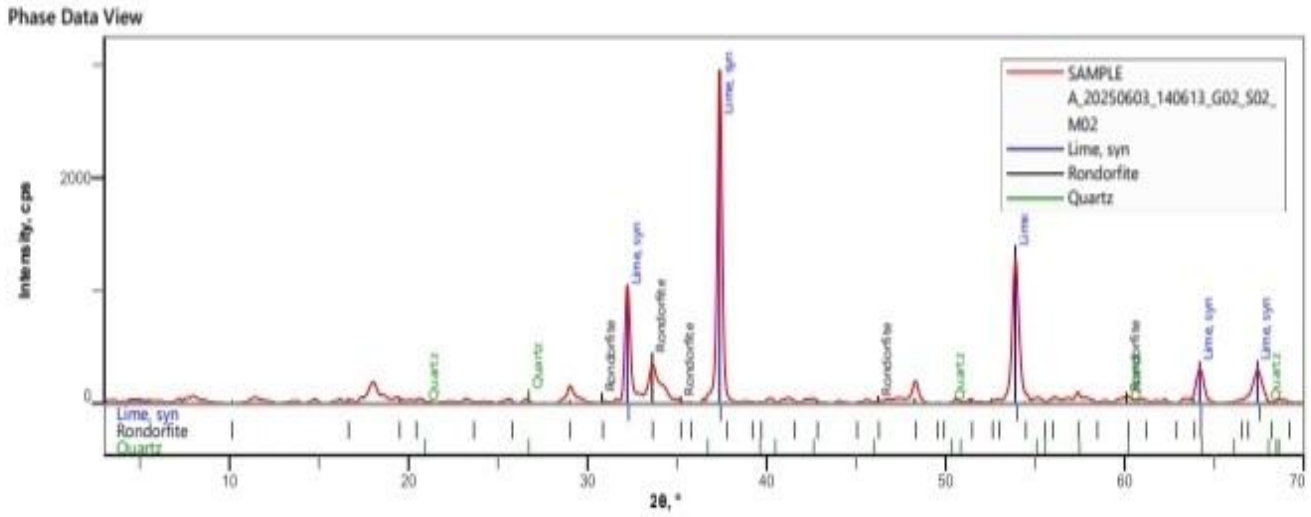

Figure 2: XRD pattern of carbide slag precursor

ISSN No. 2454-6194 | DOI: 10.51584/IJRIAS |Volume XI Issue III March 2026

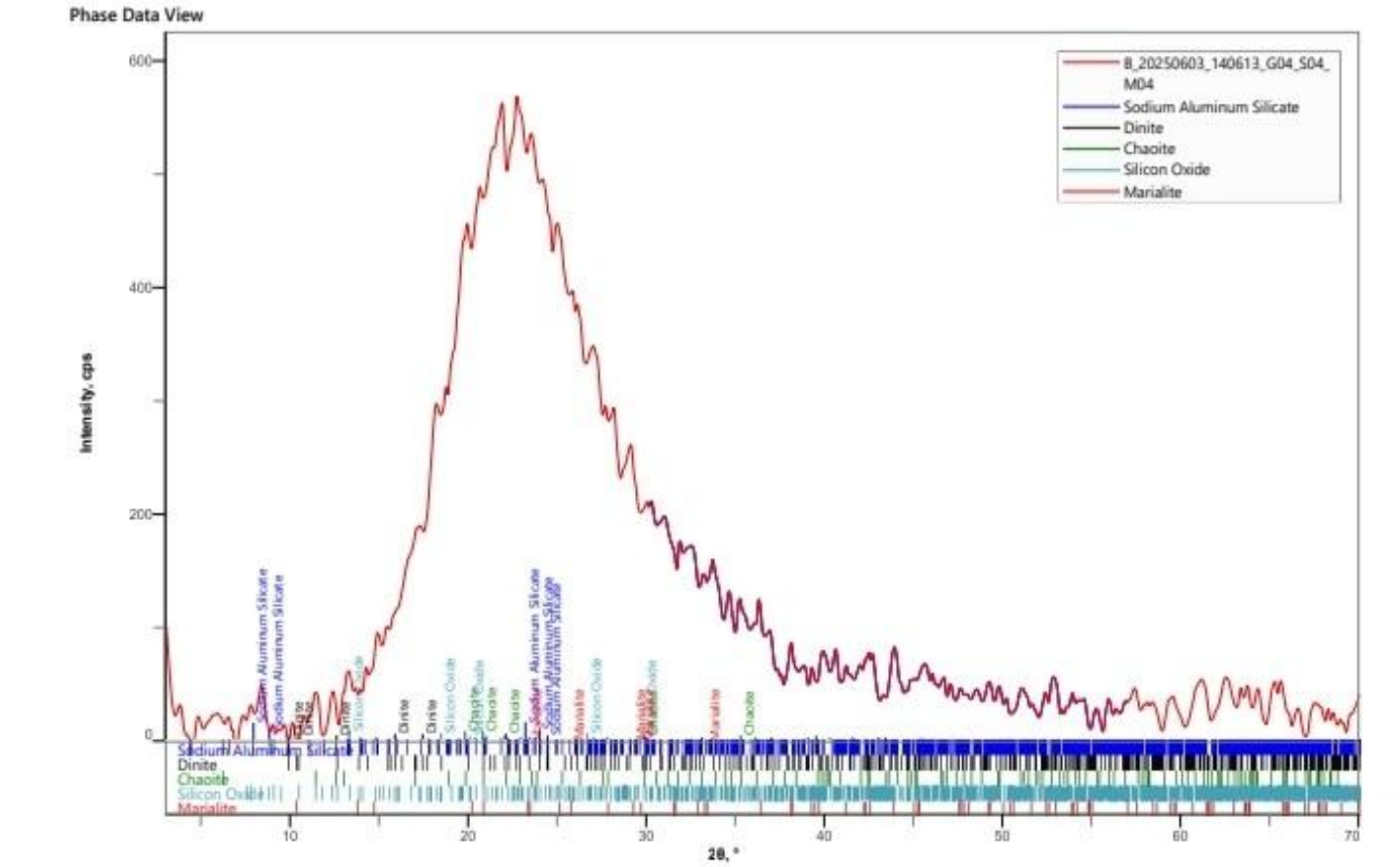

Figure 3: XRD pattern of THC precursor

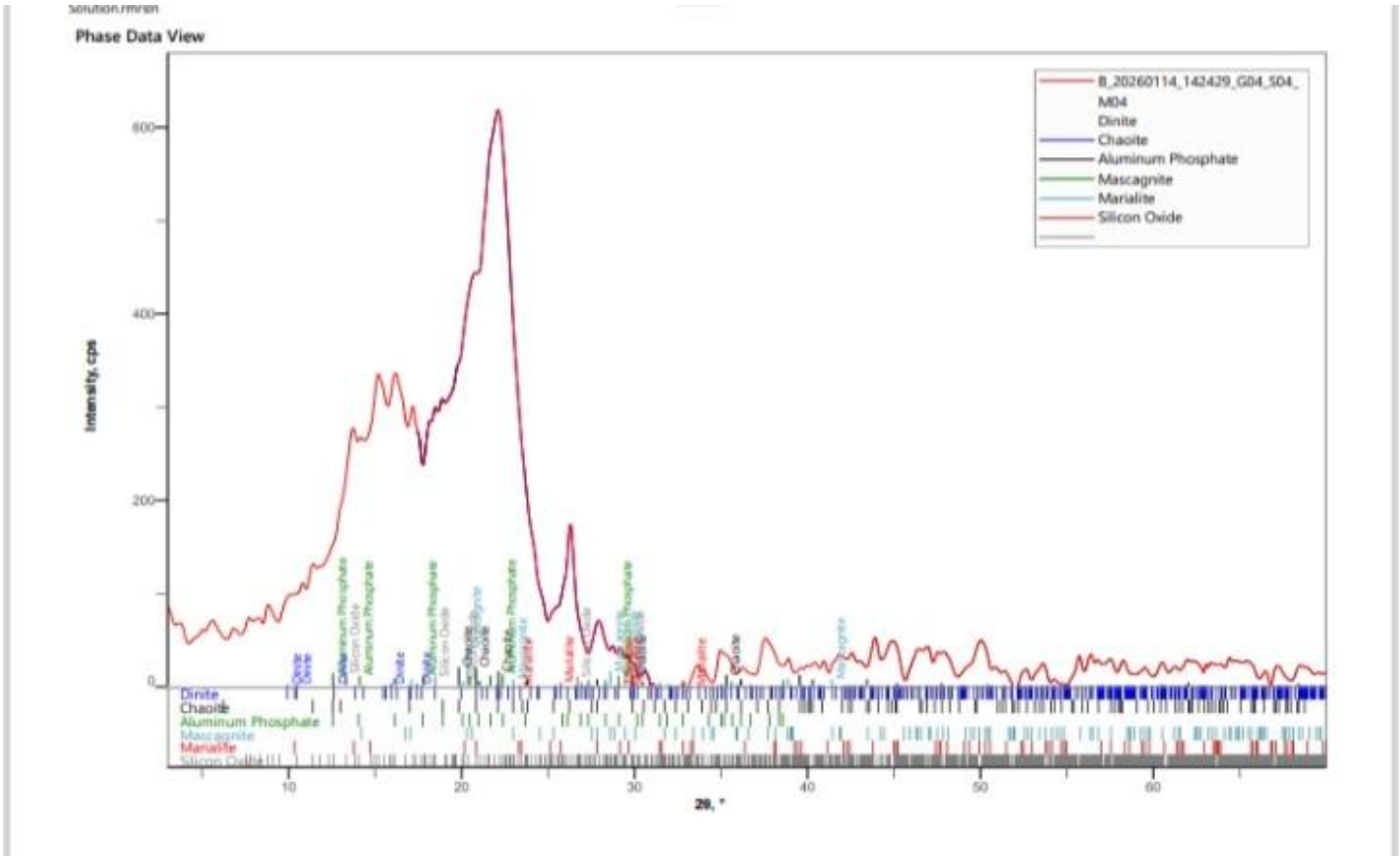

Figure 4: XRD pattern of composite catalyst before use

ISSN No. 2454-6194 | DOI: 10.51584/IJRIAS |Volume XI Issue III March 2026

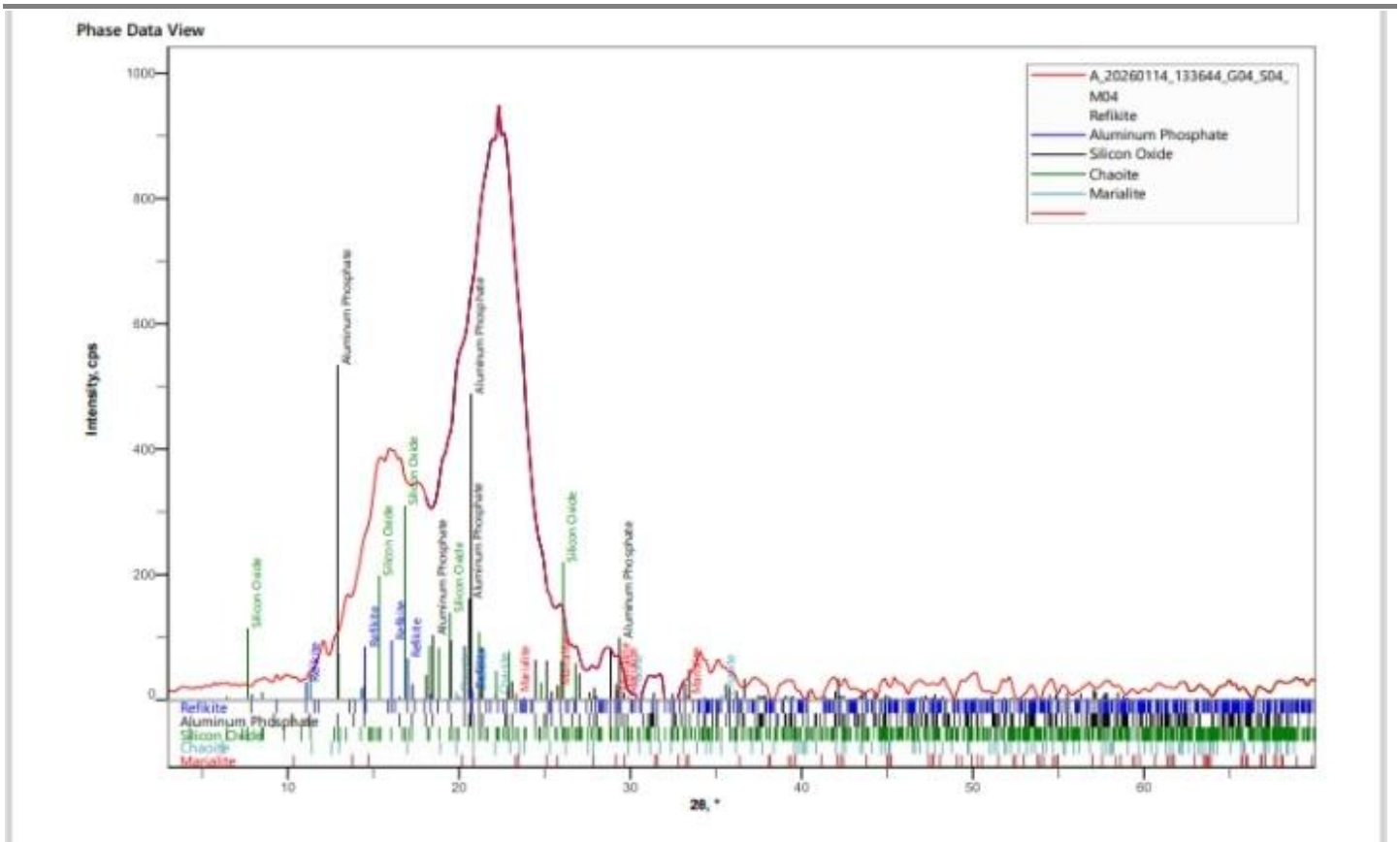

Figure 5: XRD pattern of composite catalyst after use

Brunauer-Emmett-Teller (BET) analysis

The Brunauer-Emmett-Teller (BET) analysis was conducted to quantitatively ascertain the surface characteristics of the precursors and composite catalyst before and after use. Information on their surface area, pore diameter and pore volume were obtained from the analysis as displayed on table 4. It was observed that the CARBIDE SLAG precursor had a surface area of 221.643 m^2/g, a pore diameter of 2.940 nm, and a pore volume of 0.202 cc/g, while the THC precursor had a surface area 314.180 m^2/g, a pore diameter of 2.800nm, and a pore volume of 0.283 cc/g. The surface area, pore diameter, and pore volume of the composite catalyst before use were found to be 226.888 m^2/g, 2.940 nm, and 0.207 cc/g respectively. For the composite catalyst after use, 165.708 m^2/g, 2.700 nm, and 0.103 cc/g were obtained as the surface area, pore diameter, and pore volume respectively.

As expected, the surface area of the composite catalyst typically lies between the surface area of the two precursors. This can be attributed to the blockage of some micropores by the carbide slag. It was observed that the pore diameter of the carbide slag was retained by the composite catalyst. This shows that the carbide slag precursor dominated the architecture and its pore network remained intact during the mixing, impregnation and calcination processes. The precursor with smaller pores does not collapse or occupy the larger ones. Hence the THC precursor, which was the precursor with the smaller pores in this case, did not collapse or occupy the carbide slag precursor pores. Thus, the composite's average diameter reflected the carbide slag pores system [60].

For pore volume, combining two different porous precursors of different pore volume results in a composite pore volume which is approximately equal to the mass weighted sum of the pore volumes of the precursors, if any of the pore structures was not altered during the mixing, impregnation and calcination, and if there was no pore blockage. In this case the pore composite pore volume was found to be close to the mass weighted sum of the pore volumes of the precursors, which shows that there was no significant alteration of the pore structures during the mixing, impregnation and calcination processes.

ISSN No. 2454-6194 | DOI: 10.51584/IJRIAS |Volume XI Issue III March 2026

A decrease was observed in the surface area of the composite catalyst after use. This is attributed to the occupation of the catalyst surface active sites by unreacted triglycerides [67]. A decrease in the pore diameter and pore volume was also noted.

Table 4: Surface characteristics of precursors and composite catalyst (before and after use)

Parameter	carbide slag	THC	Composite catalyst	
			Before use	After use
Surface area (m^2/g)	221.643	314.180	226.888	165.708
Pore diameter (nm)	2.940	2.800	2.940	2.700
Pore volume (cc/g)	0.202	0.283	0.207	0.146

Scanning electron microscopy (SEM) analysis

SEM was used to observe the surface morphology of the calcined carbide slag, THC, composite catalyst before use and composite catalyst after use [40].

At magnifications of 340×, 500×, and 1000×, the SEM micrographs of the calcined carbide slag in figure 6 (a), (b), and (c) show an irregular, rough, and compact surface morphology made up of large agglomerated particles with cracked edges [54]. Due to particle sintering during high-temperature calcination, the surface appears rather solid with no visible porosity. The irregular crystal development and partial fusion of Ca-based particles, characteristic of calcined calcium-rich materials, are shown by the heterogeneous texture. The carbide slag's restricted porosity emphasizes the necessity for a support material to increase dispersion.

As displayed in figure 7 (a), (b), and (c), the calcined termite hill clay (THC) has a layered, flaky, and plate-like structure that is typical of aluminosilicate clay minerals in SEM images taken at 500×, 1000×, and 1500× magnifications. In comparison to CARBIDE SLAG, the particles are more evenly dispersed and exhibit visible micro-pores and interparticle spaces, suggesting a higher surface roughness and porosity. The clay framework's thermal resilience is confirmed by the lamellar structure that was maintained following calcination [53]. This implies that THC is an efficient support material that can improve the dispersion and stabilization of Ca-based active species due to its porous and layered shape.

Prior to usage, the composite catalyst's SEM micrographs at 320×, 500×, and 750× magnifications reveal a rough and varied surface morphology made up of agglomerates with uneven shapes, as shown in figure 8 (a), (b), and (c). The structure shows good dispersion of Ca-based particles over the aluminosilicate matrix, appearing loosely packed with visible interparticle gaps and pores. The rough texture and porous nature suggest the presence of accessible active sites, which are favorable for catalytic transesterification reactions.

After biodiesel production, the SEM images in figure 9 (a), (b), and (c) reveal a more compact and denser surface structure with reduced visible porosity. The particles appear more fused and agglomerated, and some pores seem partially blocked. This morphological change can be attributed to surface carbonation of Ca-based sites, partial sintering, and deposition of reaction by-products such as glycerol and organic residues during catalytic operation. These changes are consistent with partial deactivation of the catalyst after reuse.

Comparing the SEM images of the catalyst before use and after use, surface densification and pore blockage happened during the production of biodiesel, which could have lowered the availability of active sites and accounted for any observed decrease in catalytic activity, even though the composite catalyst maintained its overall structural integrity after use.

ISSN No. 2454-6194 | DOI: 10.51584/IJRIAS |Volume XI Issue III March 2026

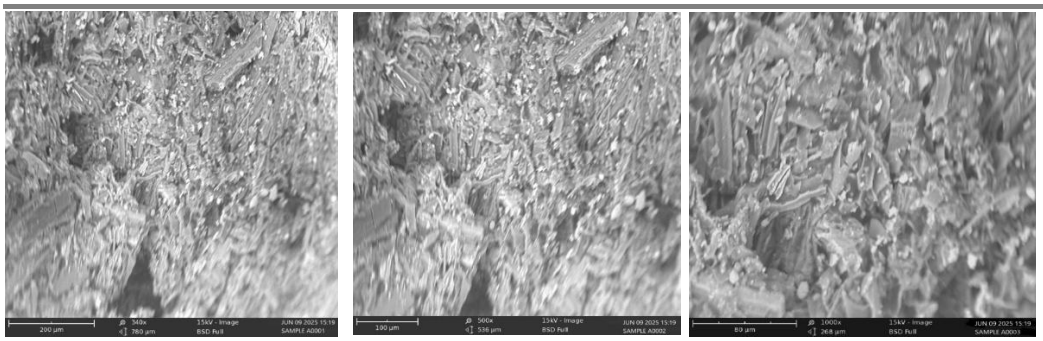

Figure 6: SEM images of carbide slag precursor (a) x340 (b) x500 (c) x1000

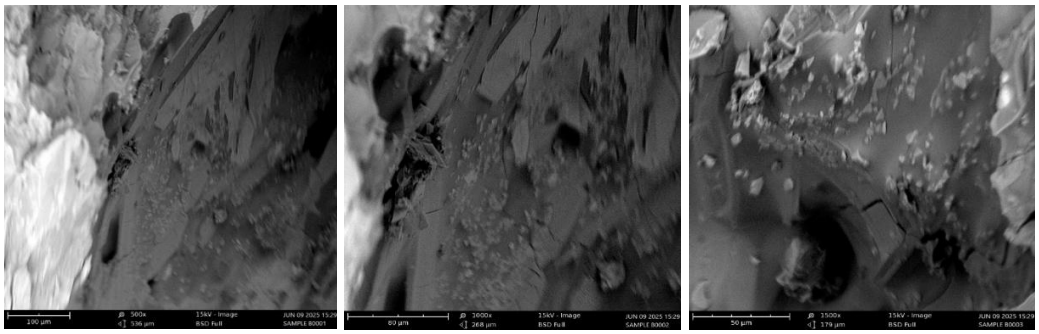

Figure 7: SEM images of THC precursor (a) x500 (b) x1000 (c) x1500

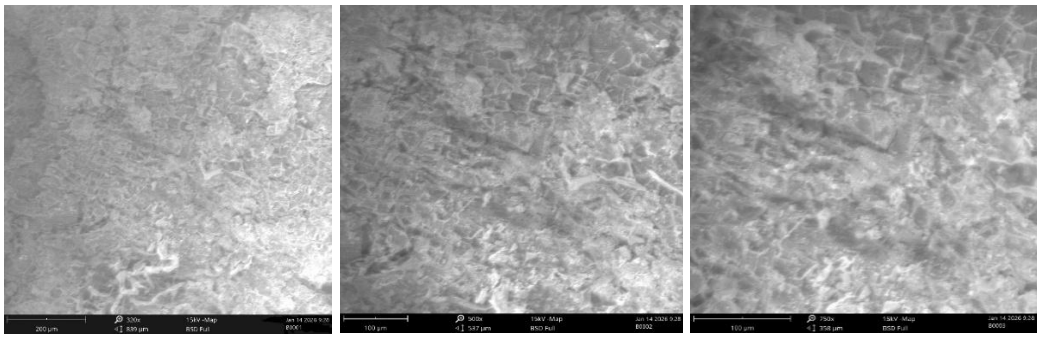

Figure 8: SEM images of composite catalyst before use (a) x320 (b) x500 (c) x750

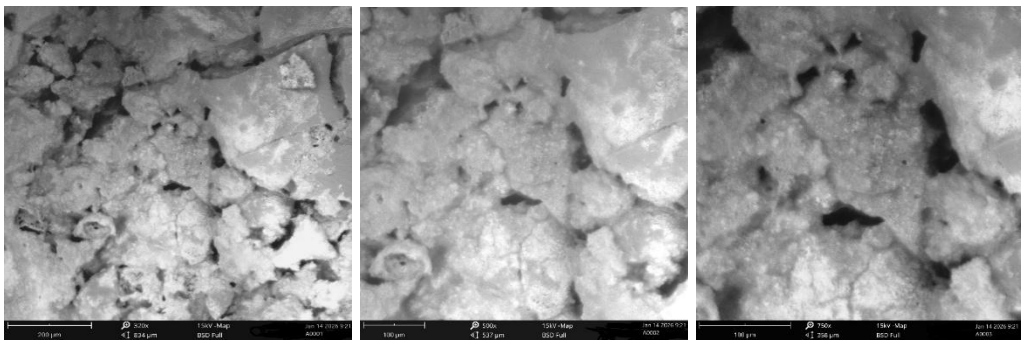

Figure 9: SEM images of composite catalyst after use (a) x320 (b) x500 (c) x750

Fourier transform infrared (FTIR) spectroscopy analysis

The identification of different functional groups available on the precursors and prepared catalyst (both before use and after use) surfaces was carried out using Fourier transform infrared (FTIR) analysis and the results are displayed below in figure 10 to figure 13. Various absorption peaks which correlate with various functional groups were indicated on the precursors and catalyst surface. The functional groups indicated by the peaks were interpreted with the aid of the Infrared Spectroscopy Absorption Table [30]. The result shown in figure 10 for the carbide slag precursor indicated a peak at 3965.9 which is typically attributed to either noise from CO_2 or

ISSN No. 2454-6194 | DOI: 10.51584/IJRIAS |Volume XI Issue III March 2026

water vapor in the air or instrument, or as a very weak, perhaps erroneous signal. Major peaks at 3906.3, 3872.7, 3842.9 and 3641.6 were attributed to the stretching of the O-H bond. A peak at 2816.0 was attributed to the stretching of the C-H bond, while the peak at 2346.4 was attributed to the stretching of the O=C=O bond. The peak at 2176.8 was attributed to the stretching of the C≡C bond. The peaks at 2104.1, 2079.9, 2027.7 and 1996.0 were attributed to the stretching of the N=C=S bond. The peaks at 1973.6, 1953.1, 1938.2 and 1917.7 were attributed to the stretching of the C=C=C bond. The peak at 1607.7 was attributed to the stretching of the C=C bond. The peak at 1559.9 was attributed to the stretching of the N-O bond. The peak at 1407.1 was attributed to the stretching of the S=O bond. The peak at 1131.2 was attributed to the stretching of the C-O bond. The peaks at 948.6, 930.0, 877.8 and 702.6 were attributed to the bending of the C-C bond while the peak at 663.5 was attributed to the stretching of the C-Br bond.

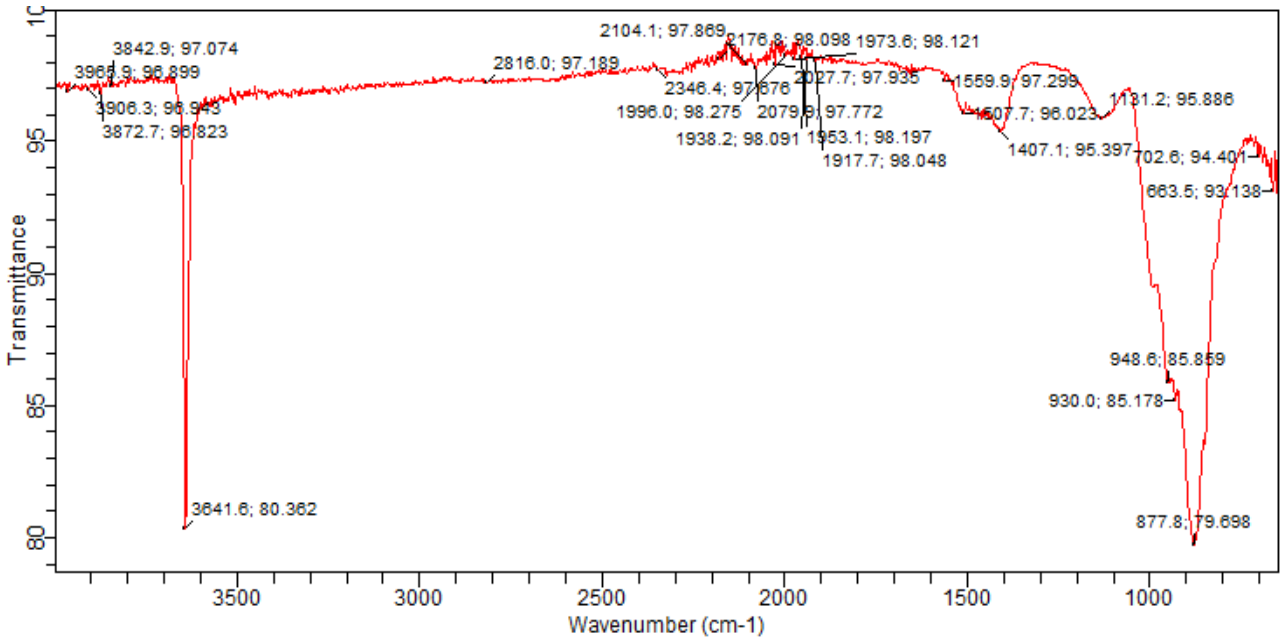

Figure 10: FTIR spectra of carbide slag precursor

The result displayed in figure 11 for THC precursor shows major peaks at 3718.0 and 3557.7, which were attributed to the stretching of the O-H bond. The peak at 3418.1 was attributed to the stretching of the N-H bond, while the peak at 2488.0 indicated a triple bond region of C≡C. Peaks at 1943.8, 2010.9, and 2079.9 were attributed to the stretching of N=C=S bond. The peak at 663.5 was attributed to the stretching of C-Br bond and the peak at 693.3 was attributed to the bending of the C=C bond, while the peak at 1071.6 was attributed to the stretching of the C-O bond.

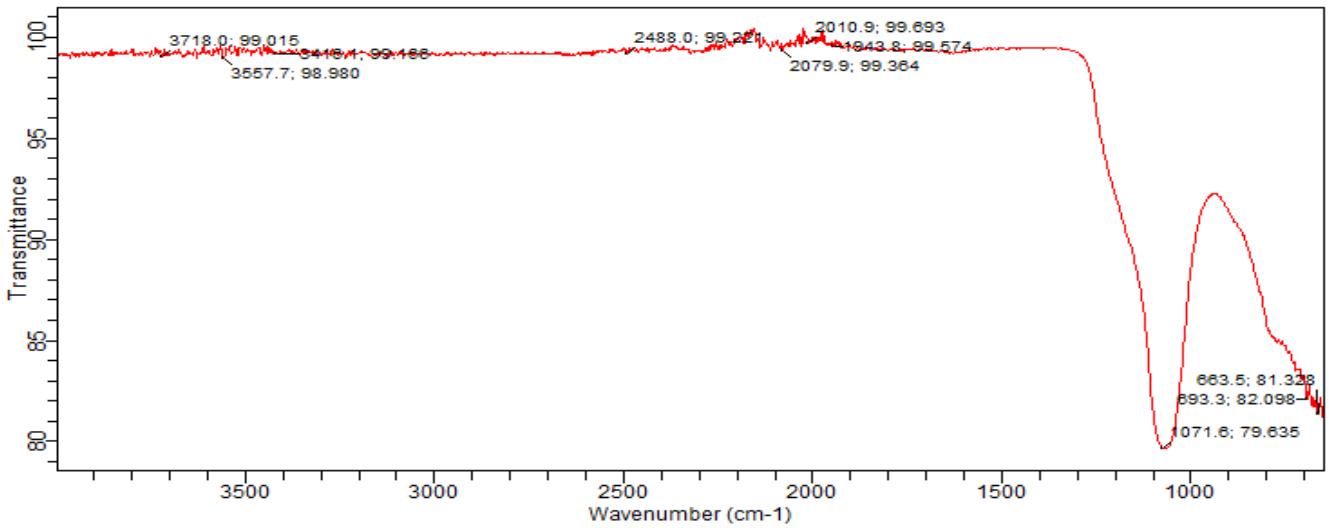

Figure 11: FTIR spectra of THC precursor

ISSN No. 2454-6194 | DOI: 10.51584/IJRIAS |Volume XI Issue III March 2026

The result displayed in figure 12 for the composite catalyst before use, shows major peaks at 3689.97 and 3619.61, which were attributed to the O-H bond stretching. The peaks at 1028.30 and 1004.06 were attributed to the stretching of the C-O bond while the peaks at 910.80 and 680.86 were attributed to the C=C bond bending. Peaks at 788.41 and 749.74 corresponded to the bending of the C-H bond while the peak at 530.24 corresponded to the bending vibrations of the Si-O-Al bond.

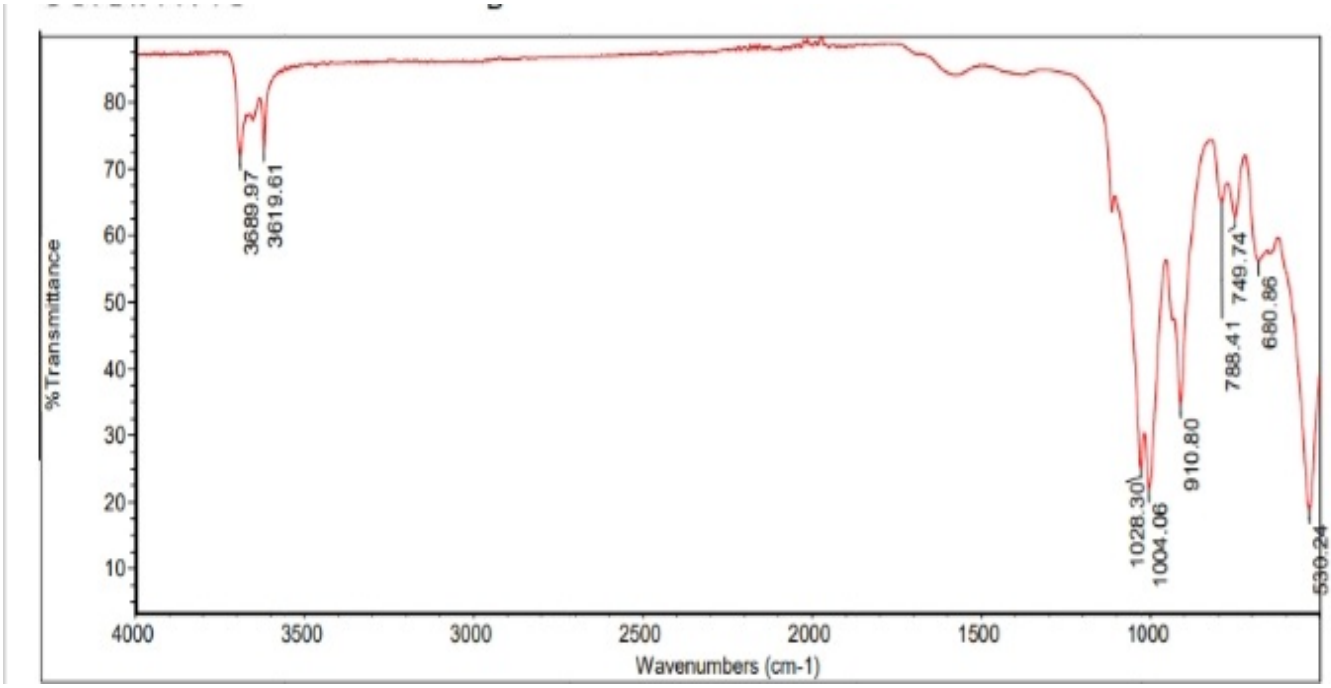

Figure 12: FTIR spectra of composite catalyst before use

Figure 13 shows the FTIR spectra of the composite catalyst after use. The different adsorption peaks identified were at 3084.15, 1979.50, 1577.88, 1058.30 and 791.95 and they corresponded to the O-H bond stretching, C-H bond bending, stretching of the C=C bond, stretching of the C-O bond and bending of the C=C bond respectively.

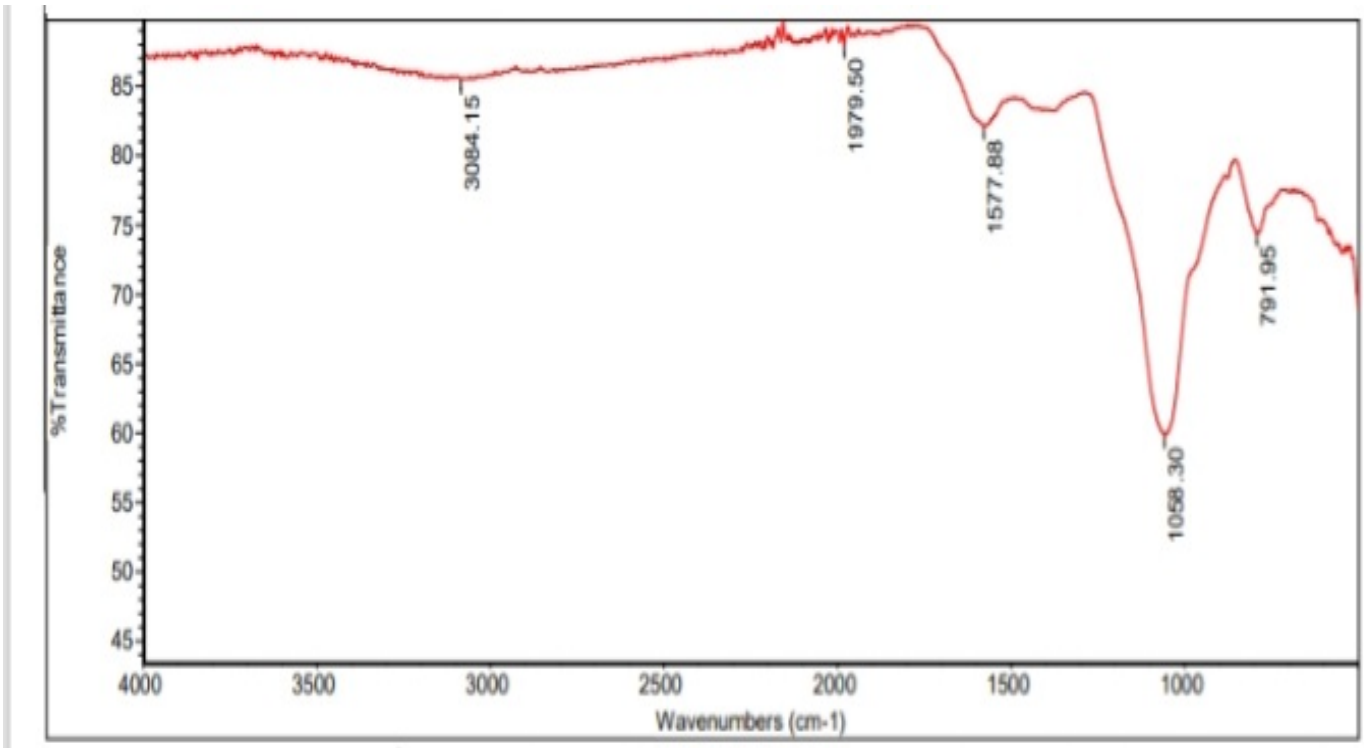

Figure 13: FTIR spectra of composite catalyst after use

ISSN No. 2454-6194 | DOI: 10.51584/IJRIAS |Volume XI Issue III March 2026

Optimization using RSM

The statistical analysis of the biodiesel production using the synthesized catalyst was carried out after generating experimental runs with Box-Behnken, performing the experiment, and inputting their respective yields. The biodiesel actual yield and their predicted values are shown in table 5. The predicted biodiesel yield was obtained using equation 3. It was noticed that similar values were obtained for both predicted and experimental results. This validates the statistical model developed for the prediction of the biodiesel yield.

$$Biodiesel\ yield\ [\%] = -618.85 + 11.63X_1 + 3.45X_2 + 12.48X_3 + 58.43X_4 - 0.0185X_1X_2 - 0.0735X_1X_3 - 0.3996X_1X_4 - 0.0504X_2X_3 - 0.1918X_2X_4 - 0.7517X_3X_4 - 0.0569X_1^2 - 0.0060X_2^2 + 0.0095X_3^2 - 1.3397X_4^2 \quad (3)$$

Table 5: Experimental and RSM predicted results for biodiesel yield

Run	Factors								Response	
	Coded values				Actual values				Biodiesel yield (%)	
	X_1	X_2	X_3	X_4	X_1	X_2	X_3	X_4	Experimental observation	RSM prediction
1	0	1	0	-1	65	120	9	1	97.96	96.90
2	1	0	0	1	70	90	9	6	79.58	78.17
3	0	-1	0	1	65	60	9	6	89.46	89.81
4	-1	0	-1	0	60	90	6	3.5	87.91	85.65
5	0	1	1	0	65	120	12	3.5	87.09	86.19
6	-1	0	0	-1	60	90	9	1	76.03	77.78
7	0	-1	-1	0	65	60	6	3.5	78.36	79.59
8	-1	-1	0	0	60	60	9	3.5	78.82	79.41
9	-1	0	1	0	60	90	12	3.5	91.54	92.09
10	0	0	0	0	65	90	9	3.5	92.56	92.76
11	0	0	-1	-1	65	90	6	1	78.67	79.08
12	0	0	1	-1	65	90	12	1	95.31	94.59
13	1	-1	0	0	70	60	9	3.5	90.06	90.06
14	1	0	0	-1	70	90	9	1	91.54	92.88
15	-1	0	0	1	60	90	9	6	84.05	83.04
16	-1	1	0	0	60	120	9	3.5	86.93	87.32
17	0	-1	0	-1	65	60	9	1	67.47	65.76
18	0	1	-1	0	65	120	6	3.5	90.25	91.03
19	0	0	1	1	65	90	12	6	78.62	78.59
20	1	1	0	0	70	120	9	3.5	87.09	86.89
21	0	1	0	1	65	120	9	6	62.41	63.41
22	1	0	-1	0	70	90	6	3.5	94.23	92.97
23	0	0	0	0	65	90	9	3.5	92.64	92.76
24	0	-1	1	0	65	60	12	3.5	93.34	92.89
25	0	0	0	0	65	90	9	3.5	91.97	92.76
26	0	0	0	0	65	90	9	3.5	93.56	92.76
27	1	0	1	0	70	90	12	3.5	93.45	94.99
28	0	0	-1	1	65	90	6	6	84.53	85.63
29	0	0	0	0	65	90	9	3.5	93.08	92.76

The quadratic model displayed remarkable fitting and predictive capabilities, leading to its recommendation as the most suitable model. The elevated R^2 value of 0.9854 signifies that more than 98% of the overall variability

ISSN No. 2454-6194 | DOI: 10.51584/IJRIAS |Volume XI Issue III March 2026

in the response is accounted for by the model. The close alignment between the adjusted R^2 (0.9707) and predicted R^2 (0.9187) confirms the model's strong predictability, while the low standard deviation (1.45) and the lowest PRESS value (163.38) among the non-aliased models further substantiate its reliability. Even though the cubic model produced an exceptionally high R^2 value of 0.9985 and a low standard deviation of 0.7025, it was identified as being aliased, which suggests confounding between model terms. As a result, in spite of its seemingly good fit, the cubic model is statistically questionable and not appropriate for additional analysis. Table 6 below displays the model summary for biodiesel yield.

Table 6: Model Summary for Biodiesel Yield

Source	Standard Deviation	R^2	Adjusted R^2	Predicted R^2	PRESS	Remark
Linear	8.64	0.1075	-0.0413	-0.3500	2712.13	
2FI	5.87	0.6911	0.5195	0.1953	1616.51	
Quadratic	1.45	0.9854	0.9707	0.9187	163.38	Suggested
Cubic	0.7025	0.9985	0.9931	0.8885	223.98	Aliased

As displayed in table 7 below, the Lack of Fit F-value of 7.88 implies the Lack of Fit is significant relative to the pure error. Its p value of 0.0308 (p value < 0.05) further shows its significance. The Model F-value of 67.33 implies the model is significant. For individual model terms, p values less than 0.05 indicate model terms are significant. When a model term is considered significant, it means that changing its value will significantly impact the response's value. For non-significant model terms, the opposite is the case [62]. In this case X_1, X_2, X_3, X_4, X_1X_2, X_1X_4, X_2X_3, X_2X_4, X_3X_4, X_1^2, X_2^2, and X_4^2were significant while X_1X_3 and X_3^2, the terms representing the interaction between reaction temperature and methanol to oil ratio and the quadratic model term representing the methanol to oil ratio, were not significant. This suggests that the biodiesel yield will be significantly impacted by changes in the values of all other model terms other than these two.

Table 7: ANOVA for the Response Surface Quadratic Model

Source	Sum of Squares	Degree of freedom	Mean Square	F-value	p-value
Model	1979.55	14	141.40	67.33	< 0.0001
X_1	78.39	1	78.39	37.33	< 0.0001
X_2	16.85	1	16.85	8.02	0.0133
X_3	53.76	1	53.76	25.60	0.0002
X_4	66.88	1	66.88	31.85	< 0.0001
X_1X_2	30.69	1	30.69	14.62	0.0019
X_1X_3	4.86	1	4.86	2.32	0.1504
X_1X_4	99.80	1	99.80	47.52	< 0.0001
X_2X_3	82.26	1	82.26	39.17	< 0.0001
X_2X_4	827.71	1	827.71	394.15	< 0.0001
X_3X_4	127.13	1	127.13	60.54	< 0.0001
X_1^2	13.14	1	13.14	6.26	0.0254
X_2^2	190.68	1	190.68	90.80	< 0.0001
X_3^2	0.0476	1	0.0476	0.0227	0.8825
X_4^2	454.76	1	454.76	216.55	< 0.0001
Residual	29.40	14	2.10		
Lack of Fit	27.98	10	2.80	7.88	0.0308
Pure Error	1.42	4	0.3552		
Corrected Totals	2008.95	28			

The goodness-of-fit statistics for the RSM model generated to forecast biodiesel yield are shown in Table 8. High experimental precision and good reproducibility of the reaction are indicated by the low coefficient of

ISSN No. 2454-6194 | DOI: 10.51584/IJRIAS |Volume XI Issue III March 2026

variation (1.68%) and standard deviation (1.45) [38]. The close agreement between the adjusted R^2 (0.9707) and predicted R^2 (0.9198) validates good model dependability and predictive capabilities, while the high coefficient of determination (R^2 = 0.9854) indicates that the model explains the great majority of the variability in biodiesel yield [39]. Additionally, the model is sufficient for navigating the design space and optimizing biodiesel yield, as seen by the outstanding signal-to-noise ratio and the suitable precision value of 32.14, which is significantly higher than the desired minimum of 4.

Table 8: Goodness of fit statistics for RSM model representing biodiesel yield

Parameter	Value
Standard Deviation	1.45
Mean	86.50
C.V. %	1.68
R^2	0.9854
Adjusted R^2	0.9707
Predicted R^2	0.9198
Adequate Precision	32.1352

Excellent agreement between model predictions and experimental values is indicated by the data points lying close to the 45° reference line in the parity plot of expected versus actual biodiesel yield as shown in figure 14. This shows that the RSM model has good prediction power and accurately depicts the system's behavior. Small variations from the line have little effect on the model's overall dependability.

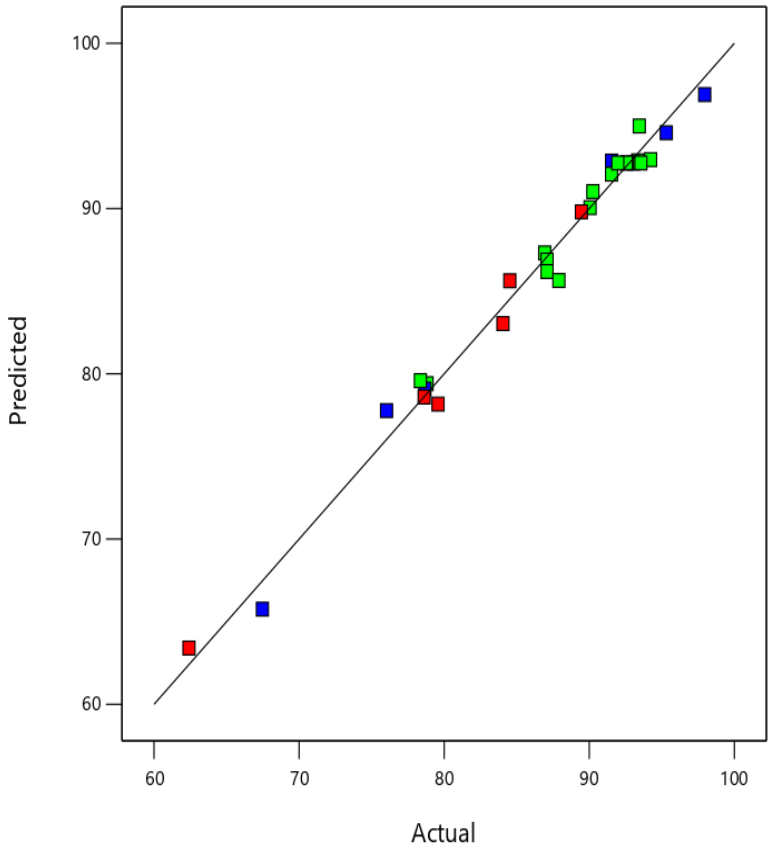

Figure 14: Parity plot comparing experimental and RSM predicted biodiesel yield

Effect of process variables on biodiesel yield

ISSN No. 2454-6194 | DOI: 10.51584/IJRIAS |Volume XI Issue III March 2026

As shown in figure 15a, the yield of biodiesel increases noticeably when the reaction temperature is raised. The yield is comparatively poor at lower temperatures, which is explained by a lack of kinetic energy necessary for efficient mass transfer and reaction completion. The yield significantly improves and reaches its maximum as the temperature rises toward higher range. Better contact between reactants, decreased viscosity of the reaction mixture, and enhanced reaction kinetics are probably the causes of this improvement [59]. In agreement with the principles of Arrhenius equation, biodiesel yield is favoured at higher temperatures as an increase in reaction rates is predicted with an increase in temperature [14]. Previous studies showed corresponding pattern of increase in biodiesel yield with reaction temperature [24]; [50]. It is observed that forward reaction is also favoured when reaction time is increased. The increase in biodiesel yield with increase in reaction time is as a result of conversion of triglycerides available in the oil to fatty acid methyl esters, which is the major composition of biodiesel product [28].

An important interaction between reaction temperature and reaction time is suggested by the elliptical contour pattern seen at the surface's base. The yield tends to plateau outside of the ideal range, suggesting that equilibrium conditions are near and that additional temperature or time increases do not significantly improve conversion efficiency. These results show that in order to maximize the production of biodiesel, reaction temperature and reaction time both play crucial synergistic roles.

The combined effects of reaction temperature and methanol-to-oil ratio on biodiesel yield when examined within the experimental range is shown in figure 15b. The surface shows a primarily linear rising trend, suggesting that both variables have a favorable impact on biodiesel production. Because of improved mass transfer between reactants, decreased oil viscosity, and improved reaction kinetics, the yield of biodiesel gradually rises as the reaction temperature rises [3]. According to Le Chatelier's principle, raising the methanol-to-oil ratio also encourages the formation of ester by moving the reversible transesterification reaction in the direction of product formation [16]. The comparatively straight contour lines at the surface's base point to a weak interaction effect between the methanol-to-oil ratio and temperature, suggesting that their contributions to the yield of biodiesel are mostly additive rather than highly synergistic. Higher Temperatures and methanol-to-oil ratios provide ideal kinetic and equilibrium conditions for effective conversion, resulting to high yield. However, yield may not be appreciably increased by exceeding the ideal range of methanol ratios, and downstream separation procedures may become more difficult [15]

The interactions between catalyst loading and reaction temperature on biodiesel yield is illustrated by the three-dimensional response surface plot in figure 15c. Catalyst loading has a noticeable quadratic effect, raising yield from 1 weight percent to about 4–5 weight percent, after which it only slightly improves. This effect is explained by the fact that adequate doses increase the number of active catalytic sites accessible, hence improving the efficiency of triglyceride conversion [20].

Excessive catalyst loading, however, may limit further yield improvement by increasing mixture viscosity, leading to soap formation, and making product separation challenging [33]; [65]. The plot's curved contour lines show a moderate interaction between temperature and catalyst loading, indicating that the catalytic effect intensifies at higher temperatures as a result of increased molecule collision frequency and reaction rate [23]. At temperatures close to 70°C and catalyst loading between 4 and 5 weight percent, the best biodiesel yield of about 98% is obtained, suggesting ideal kinetic and catalytic conditions for effective transesterification.

The 3 D surface plot in figure 15d indicates that the production of biodiesel is significantly influenced by the ratio of methanol to oil. As the ratio grows near 12:1, the yield increases dramatically, demonstrating that additional methanol leads to increase in yield. At lower ratios, around 6:1, the yield stays small. This discovery is consistent with research that indicates a higher methanol-to-oil ratio improves the efficiency of transesterification and the production of biodiesel [15]. Reaction time is also a significant factor. While shorter reaction time of around 60 minutes produce lower yields, longer reaction times of more than 90 minutes enable the process to attain completion and increase yield. Longer reaction time and enough methanol produce higher yields, frequently surpassing 85–90%, according to previous research [35].

The 3 D surface plot in figure 15e illustrates how catalyst loading and reaction time affect biodiesel yield. Even with prolonged reaction time, yields are still small at low catalyst loadings (around 1 wt %). The yield

ISSN No. 2454-6194 | DOI: 10.51584/IJRIAS |Volume XI Issue III March 2026

dramatically increases as catalyst loading approaches 4 wt%, showing that more catalyst speeds up transesterification and increases yield. This is in line with research by Masango et al. [35] that found that higher catalyst concentrations increase the efficiency of biodiesel production. Another important factor is reaction time. Shorter reaction times (about 60 minutes) result in lower yields, whereas longer reaction time (above 90 minutes) enable the reaction to proceed further and provide higher yields. This is consistent with previous studies that showed that yields above 85–90% are achieved when longer reaction times are paired with an adequate amount of catalyst [64].

This 3D response surface plot in figure 15f illustrates how the methanol-to-oil ratio and catalyst loading interact to affect the yield of biodiesel. Even when the methanol-to-oil ratio is raised, yields are still small at low catalyst loadings (around 1 wt%). The yield dramatically improves as catalyst loading increases toward 4 wt%, demonstrating that additional catalyst speeds up the transesterification reaction and increases conversion efficiency and yield. This discovery is in line with research showing that increased catalyst concentrations increase the efficiency of biodiesel production [61]. Likewise, as additional methanol propels the process toward completion, raising the methanol-to-oil ratio from 6:1 to 12:1 increases yield. Optimizing the methanol-to-oil ratio is essential for improving the yield of biodiesel, according to previous studies [15]. Additionally, studies show that in order to achieve high conversion rates without using too much reagent, the methanol ratio and catalyst concentration need to be balanced [6].

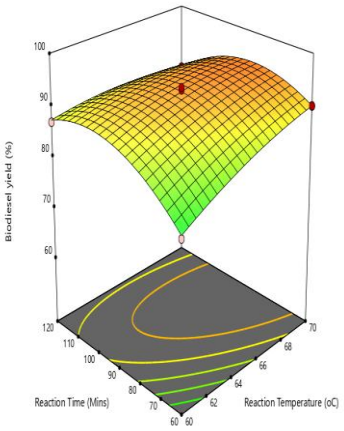

(a)

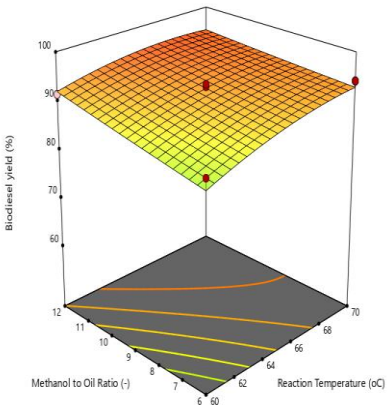

(b)

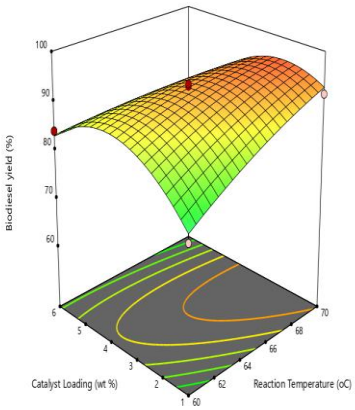

(c)

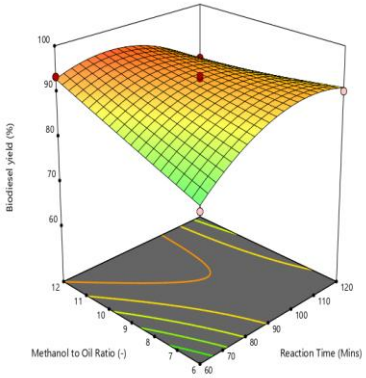

(d)

ISSN No. 2454-6194 | DOI: 10.51584/IJRIAS |Volume XI Issue III March 2026

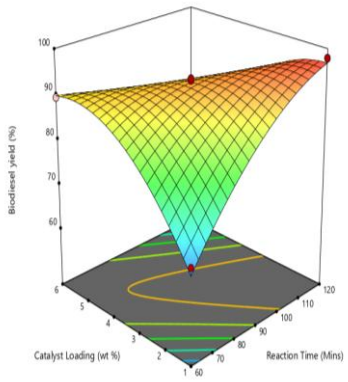

(e)

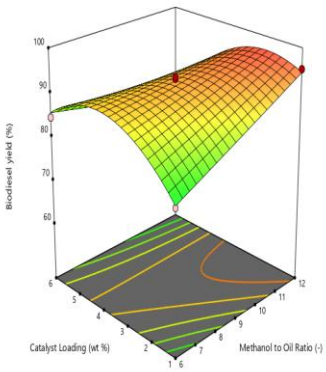

(f)

Figure 15: 3D surface plots showing interaction between (a) temperature and time (b) temperature and methanol: oil ratio (c) temperature and catalyst loading (d) time and methanol: oil ratio (e) time and catalyst loading (f) methanol: oil ratio and catalyst loading

Numerical optimization

From the numerical optimization, the optimum biodiesel yield was obtained as 98.22% at a reaction temperature of 66.95 ^{o}C, a reaction time of 94.04 mins, methanol to oil ratio of 11.98:1, and catalyst loading of 2.39 wt%. The desirability value for this achievement was one (1), which is an indication that the optimal values were totally acceptable. These results obtained from optimization were verified in the laboratory by carrying out 3 runs of biodiesel production with the optimal values and computing the average of the biodiesel yields obtained from the different runs. The average biodiesel yield was obtained as 98.16%, which is not too far from the predicted optimum biodiesel yield of 98.22%. Table 9 displays the comparison of the optimum experimental conditions and optimum yield obtained from this study with past studies.

Table 9: Comparison of optimum experimental conditions and optimum yield with past studies

Feedstock	Catalyst source	Reaction temperature (^{o}C)	Reaction time (mins)	Methanol to oil ratio	Catalyst loading (wt%)	Biodiesel yield (%)	Reference
Bauhinia monandra oil	Banana peel	65	69.02	7.6:1	2.75	98.5	[8]
Waste cooking oil	KBr/CaO	65	109.8	12:1	3	83.6	[49]
Waste cooking oil	Crab shell and plantain peel	60	149.94	13.03:1	5	93.0	[4]
Waste vegetable oil	NI-Sr-doped CaO	74.86	119.92	11.41:1	5.12	98.0	[43]
Castor oil	K2CO3/γ-Al2O3	70	180	9:1	3	94.3	[56]
Podocarpus falcatus seed oil	CaO/CeO2	63.2	91.2	11.82:1	1.59	98.32	[9]
P. K. O	Carbide slag/ Termite hill Clay	66.95	94.04	11.98:1	2.39	98.22	This study

ISSN No. 2454-6194 | DOI: 10.51584/IJRIAS |Volume XI Issue III March 2026

Catalyst Reusability Studies

In the first run, the biodiesel yield was obtained as 98.2%. The second run gave a biodiesel yield of 92.4%, while the third run gave a biodiesel yield of 84.5%. the fourth, fifth and sixth runs gave biodiesel yields of 81.3%, 74.9%, and 69.8% respectively, as Figure 16 illustrates. Progressive reductions in biodiesel yields were observed as the number of cycles increased. There was an overall reduction of 28.4% in biodiesel yield between the first and sixth run. One possible explanation for the decrease in biodiesel production is that unreacted triglycerides are increasingly occupying the catalyst's surface active sites, which gradually reduces the catalyst's effectiveness [4]; [67]. Some other researchers who studied the reusability of heterogeneous catalysts for the production of biodiesel reported similar findings [70].

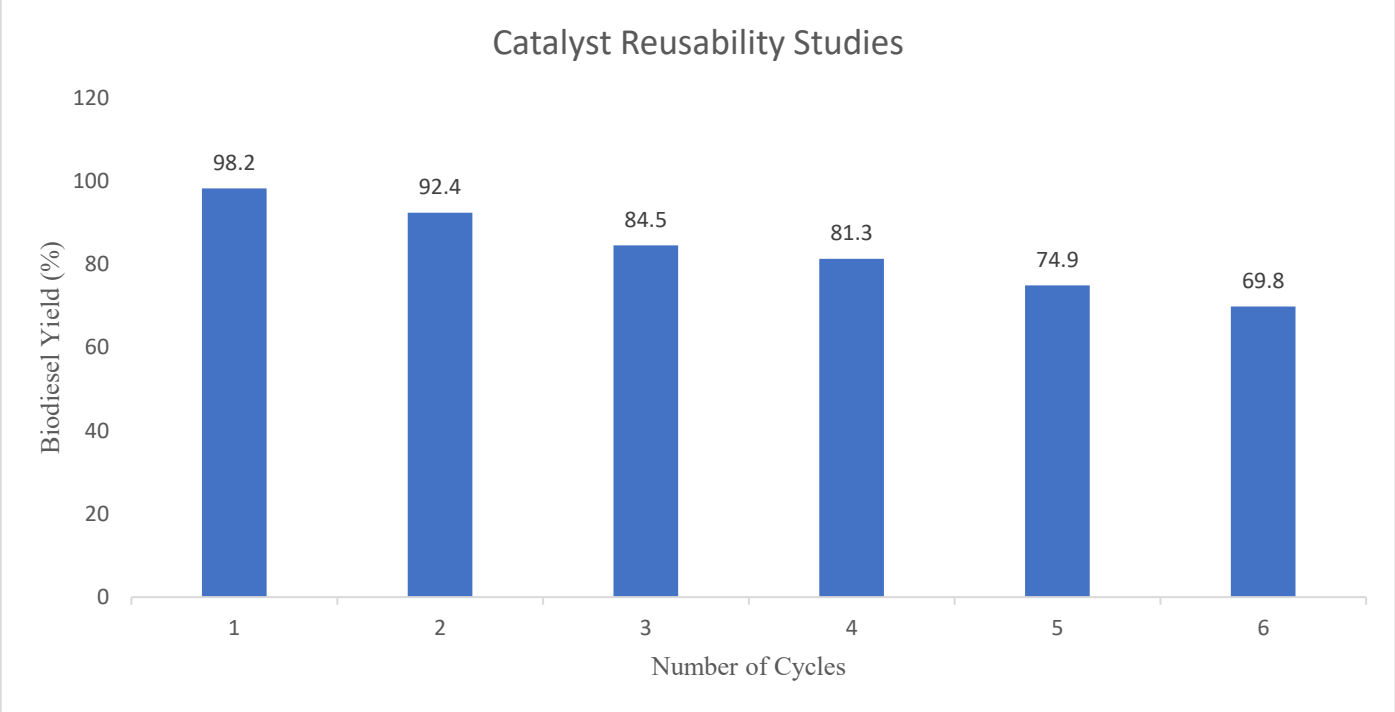

Figure 16: Catalyst reusability studies results

Characterization of Biodiesel

Comparison was carried out between the characteristics of the produced biodiesel at the optimized conditions and the ASTM D6571 and EN 14214 standards and the results are shown in Table 10. There is agreement between the results obtained and the ASTM D6571 and EN 14214 standards. The density was obtained as 0.863g/cm$^{3.}$ The recommended acid value is <0.5 and the acid value of the produced biodiesel was determined as 0.266 mgKOH/g. This low value is an indication that there will be little or no corrosion problems associated with using the biodiesel as fuel [66]. The FFA was obtained as 0.133%, while the sap value was gotten as 206.44 mgKOH/g. The iodine value was determined as 23.5 I_2/100g, while the viscosity was found to be 3.60 mPa.s at 40ºC, 30.0 RPM, 18.0%. The pour point, flash point and cloud point were determined as -5 ºC, 179 ºC and -6 ºC respectively, while the cetane number and higher heating value were obtained as 67.44 and 40.64 respectively.

Table 10: Properties of biodiesel

Properties	**Biodiesel**	**ASTM D6751**	**EN 14214**
Colour	Golden yellow	Not specified	Not specified
Physical state at room temperature	Liquid	Not specified	Not specified
Density (g/cm^3)	0.863	Not specified	Not specified
Acid value (mgKOH/g)	0.266	<0.5	<0.5
Free fatty acid (%)	0.133	Not specified	Not specified

ISSN No. 2454-6194 | DOI: 10.51584/IJRIAS |Volume XI Issue III March 2026

Saponification value (mgKOH/g)	206.44	Not specified	Not specified
Iodine value (I_2/100g)	23 .5	Not specified	<120
Viscosity @ 40 ºC (mPa.s)	3.6	1.9 to 6.0	3.5 to 5.0
Pour point (ºC)	-5	<0	<0
Flash point (ºC)	179	>130	>120
Cloud point (ºC)	-6	Not specified	Not specified
Cetane number	67.44	≥47	≥51
Higher heating value	40.64	Not specified	≥35
Aniline point	81	Not specified	Not specified

Table11 displays the major identified FAME Components of the produced biodiesel. The FAME was dominated by oleic acid (44.5%), lauric acid (28.17%), palmitic acid (11.3%), stearic acid (8.81%), myristic acid (0.58%), and linoleic acid (0.48%). Other non-FAME components, such as phthalates (contaminants) and squalene were detected in the sample in proportion of 0.83% and 0.64% respectively. The presence of saturated components in the sample contributes to good oxidative stability and high cetane number of the biodiesel while the presence of the monounsaturated components suggests moderate cold flow properties.

Table 11: Major Identified FAME Components (Desired Biodiesel Products)

Fatty acid	**Chemical formula**	**Nature**	**Composition (%)**
Oleic acid	$C_{18}H_{34}O_2$	Unsaturated	44.5
Lauric acid	$C_{12}H_{24}O_2$	Saturated	28.17
Palmitic acid	$C_{16}H_{32}O_2$	Saturated	11.3
Stearic acid	$C_{18}H_{36}O_2$	Saturated	8.81
Myristic acid	$C_{14}H_{28}O_2$	Saturated	0.58
Linoleic acid	$C_{18}H_{32}O_2$	Unsaturated	0.48
Phthalates (contaminants)	Various	Non-FAME	0.83
Squalene	Hydrocarbon	Unsaturated (Non-FAME)	0.64
Others			4.69
Total			100

CONCLUSION

Biodiesel was produced from palm kernel oil using an efficient heterogeneous catalyst synthesized from naturally occurring low value material and waste material (carbide slag and THC). Optimization of the biodiesel production was carried out using RSM and a high R^2 value of 0.9854 was observed, indicating that RSM can be used as an optimization tool for the biodiesel production process. This study has ascertained the optimum experimental conditions for utilizing the bifunctional composite catalyst to produce biodiesel from palm kernel oil. An optimum biodiesel yield was obtained as 98.22% at a reaction temperature of 66.95 ºC, a reaction time of 94.04 mins, methanol to oil ratio of 11.98:1, and catalyst loading of 2.39 wt%. The physicochemical properties of the biodiesel obtained using the catalyst produced was within the appropriate range of ASTM D6751 specifications for biodiesel.

ACKNOWLEDGEMENT

This study was supported by the Petroleum Technology Development Fund (PTDF), through the PTDF Professorial Chair on Renewable Energy in the Department of Chemical Engineering, University of Benin, Nigeria.

REFERENCES

1. Ajala, E. O., Ehinmowo, A. B., Ajala, M. A., Ohiro, O. A., Aderibigbe, F. A., & Ajao, A. O. (2022).

Optimisation of CaO-Al2O3-SiO2-CaSO4-based catalysts performance for methanolysis of waste lard for biodiesel production using response surface methodology and meta-heuristic algorithms. Fuel Processing Technology, 226, 107066.

2. Al-Sakkari, E. G., El-Sheltawy, S. T., Attia, N. K., & Mostafa, S. R. (2017). Kinetic study of soybean oil methanolysis using cement kiln dust as a heterogeneous catalyst for biodiesel production. Applied Catalysis B: Environmental, 206, 146–157. https://doi.org/10.1016/j.apcatb.2017.01.008
3. Alagha, S. M., & Salih, R. (2023). Review the studies of mass transfer and kinetic modeling for production the biodiesel by the transesterification method and the impact of some selected factors Review the studies of mass transfer and kinetic modeling for production the biodiesel by the tr. IOP Conference Series: Earth and Environmental Science. https://doi.org/10.1088/1755-1315/1232/1/012014
4. Amenaghawon, A. N., Obahiagbon, K., Isesele, V., & Usman, F. (2022). Optimized biodiesel production from waste cooking oil using a functionalized bio-based heterogeneous catalyst. Cleaner Engineering and Technology, 8, 100501. https://doi.org/10.1016/j.clet.2022.100501
5. Anusha, P., Janeefa, P., Gangadhara, R., & T, S. R. (2021). Biodiesel Preparation , Process Optimization and Characterization from Neem seed Oil. Int J Res Appl Sci Eng Technol, 9(10), 525–527.
6. Aremanda, R. B., Tekleweyni, D., Arebu, M., Fufa, G., & Nasir, M. (2025). Influence of Methanol Solvent and Alkali Catalyst on Biodiesel Production from Cottonseed Oil. International Journal of Energetica, 10(1), 24–30.
7. Balajii, M., & Niju, S. (2019). Biochar - derived heterogeneous catalysts for biodiesel production. Environmental Chemistry Letters, 17(4), 1447–1469. https://doi.org/10.1007/s10311-019-00885-x
8. Betiku, E., Akintunde, A. M., & Ojumu, T. V. (2016). Banana peels as a biobase catalyst for fatty acid methyl esters production using Napoleon's plume (Bauhinia monandra) seed oil: A process parameters optimization study. Energy, 103, 797–806. https://doi.org/10.1016/j.energy.2016.02.138
9. Biru Birhanu, Devendra Deshmukh, T. H. and K. Y. (2025). RSM-Optimized Biodiesel Production from Ethiopian Podocarpus falcatus Seed Oil Using a CaO-CeO_2 Stability Assessment Meaning IN IN. Scientific Reports.
10. Çapa, T., Bahç, B., & Abdeljelil, B. Ben. (2023). Assessment of Homogeneous and Heterogeneous Catalysts in Transesterification Reaction : A Mini Review. ChemBioEng, 4, 412–422. https://doi.org/10.1002/cben.202200021
11. Chumuang, N., & Punsuvon, V. (2017). Response Surface Methodology for Biodiesel Production Using Calcium Methoxide Catalyst Assisted with Tetrahydrofuran as Cosolvent. 14(1), 4190818.
12. Cordeiro, D. O., Silva, J. E., Oliveira, A. A. S., Batista, W. G. S., & Neto, E. L. B. (2019). Influence Of Carbonation And Rehydration On Cao Derived From Calcining Chicken Eggshells In The Catalytic Process Of Soybean. Brazillian Journal of Petroleum and Gas, 13(1), 5419.
13. Dolvine, N., Dongmo, S., Bruno, L., Meme, L., & Tongnang, N. (2024). Biodiesel Production From High FFA Raphia vinifera Oil as a Potential Non-edible Feedstock : Process Optimization Using Response Surface Methodology. Chemistry Africa, 7(3), 1481–1496. https://doi.org/10.1007/s42250-023-00814-0
14. Donald, P., Sanchez, C., Hashim, N., Shamsudin, R., & Mohd, M. Z. (2021). Effects of different storage temperatures on the quality and shelf life of Malaysian sweet potato (Ipomoea Batatas L .) varieties. Food Packaging and Shelf Life, 28(October 2020), 100642. https://doi.org/10.1016/j.fpsl.2021.100642
15. Ehiri, R. C. (2010). Determination of optimal methanol: oil volume ratio for maximum biodiesel production from waste cooking oil. Journal of Physical Sciences and Innovation, 2(December), 7–10.
16. Gibreel, O. H. O. (2022). Potential of Biodiesel Production from Waste Cooking Oil in Qatar: Techno-Economic Study. In (Doctoral dissertation, Manara-Qatar Research Repository).
17. Glass, S., Santiago-cruz, H. A., Chen, W., Zhang, T., Guelfo, J., Rittmann, B., Senftle, T. P., Vikesland, P., Villagrán, D., Wang, H., Westerhoff, P., Wong, M. S., Jiang, G., Lowry, G. V, & Alvarez, P. J. J. (2025). Merits , limitations and innovation priorities for heterogeneous catalytic platforms to destroy PFAS. Nature Water, 3(6), 644–654. https://doi.org/10.1038/s44221-025-00433-8
18. Gonçalves, M. A., Cristina, H., Maria, P., & Paula, A. (2024). Catalytic conversion of residual raw material into biodiesel using a superior magnetic solid acid catalyst based on Zn – Fe ferrite : thermodynamic and kinetic studies. Royal Society of Chemistry, 14, 20743–20756. https://doi.org/10.1039/d4ra03580a
19. Gupta, V., & Singh, K. P. (2023). The impact of heterogeneous catalyst on biodiesel production ; a review. Materials Today: Proceedings, 78, 364–371.

20. Ifeanyi-Nze, F. O., Omiyale, C. O., & Okonkwo, I. U. (2023). Biodiesel Synthesis from Waste Vegetable Oil Utilizing Eggshell Ash as an Innovative Heterogeneous Catalyst. Archives of Advanced Engineering Science, 1–18. https://doi.org/10.47852/bonviewAAES32021761
21. Indrianty, I. A., & Muchtar, M. (2024). Utilization Of used oil into biodiesel by using duck bone catalyst to meet the needs of diesel fuel review. In BIO Web of Conferences, 123, 04006. https://doi.org/https://doi.org/10.1051/bioconf/202412304006
22. Jambhulkar, D. K., Ugwekar, R. P., Bhanvase, B. A., & Divya, P. (2020). A review on solid base heterogeneous catalysts : preparation , characterization and applications. Chemical Engineering Communications, 209(4), 433–484. https://doi.org/10.1080/00986445.2020.1864623
23. Javed, F., Rizwan, M., Asif, M., Ali, S., Aslam, R., Akram, M. S., Zimmerman, W. B., & Rehman, F. (2022). Intensification of Biodiesel Processing from Waste Cooking Oil , Exploiting Cooperative Microbubble and Bifunctional Metallic Heterogeneous Catalysis. Bioengineering, 9(10), 533. https://doi.org/10.3390/bioengineering9100533
24. Khoobbakht, G., Kheiralipour, K., Rasouli, H., & Ra, M. (2020). Experimental exergy analysis of transesterification in biodiesel production. Energy, 196, 117092. https://doi.org/https://doi.org/10.1016/j.energy.2020.117092
25. Kingkam, W., Maisomboon, J., Khamenkit, K., Nuchdang, S., Nilgumhang, K., Issarapanacheewin, S., & Rattanaphra, D. (2024). Preparation of CaO @ CeO 2 Solid Base Catalysts Used for Biodiesel Production. Catalysts, 14(4), 240.
26. Komadel, P. (2016). Acid activated clays : Materials in continuous demand. Applied Clay Science, 131, 84–99. https://doi.org/10.1016/j.clay.2016.05.001
27. Krödel, M., Leroy, C., Kim, S. M., Naeem, M. A., Kierzkowska, A., Wu, Y.-H., Armutlulu, A., Fedorov, A., Florian, P., & Müller, C. R. (2023). Of Glasses and Crystals: Mitigating the Deactivation of CaO-Based CO 2 Sorbents through Calcium Aluminosilicates. Journal of the American Chemical Society, 3, 3111–3126. https://doi.org/10.1021/jacsau.3c00475\
28. Kumar, S. A. A., Sakthinathan, G., Vignesh, R., Banu, J. R., & Al-muhtaseb, A. H. (2019). Optimized transesterification reaction for efficient biodiesel production using Indian oil sardine fish as feedstock. Fuel, 253, 921–929. https://doi.org/10.1016/j.fuel.2019.04.172
29. Li, M., Chen, J., Li, L., Ye, C., Lin, X., & Qiu, T. (2021). ScienceDirect Novel multi – SO 3 H functionalized ionic liquids as highly efficient catalyst for synthesis of biodiesel. Green Energy and Environment, 6(2), 271–282. https://doi.org/10.1016/j.gee.2020.05.004
30. LibreTexts. (2022). Infrared Spectroscopy Absorption Table (p. 22645). https://chem.libretexts.org/@go/page/22645%0A
31. Malabadi, R. B. (2023). Biodiesel production: An updated review of evidence. International Journal of Biological and Pharmaceutical Sciences Archive, 2023, 06 (02), 110–133.
32. Malabadi, R. B., Sadiya, M. R., Kolkar, K. P., & Chalannavar, R. K. (2023). Biodiesel production via transesterification reaction. Open Access Research Journal of Science and Technology, 9(2), 010–021. https://doi.org/10.53022/oarjst.2023.9.2.0064
33. Mandari, V., & Kumar, S. (2022). Biodiesel Production Using Homogeneous , Heterogeneous , and Enzyme Catalysts via Transesterification and Esterification Reactions : a Critical Review. BioEnergy Research, 15(2), 935–961. https://doi.org/10.1007/s12155-021-10333-w
34. Mardhiah, H. H., Ong, H. C., Masjuki, H. H., Lim, S., & Lee, H. V. (2017). A review on latest developments and future prospects of heterogeneous catalyst in biodiesel production from non-edible oils. Renewable and Sustainable Energy Reviews, 67, 1225–1236. https://doi.org/10.1016/j.rser.2016.09.036
35. Masango, S. B., Ngema, P. T., & Olagunju, O. A. (2024). The Effect of Reaction Temperature , Catalyst Concentration and Alcohol Ratio in the Production of Biodiesel from Raw and Purified Castor Oil. Advances in Chemical Engineering and Science, 14, 137–154. https://doi.org/10.4236/aces.2024.143009
36. Mohamed, S., Aghareed, F., Shereen, M. T., Hamid, M. S. A., & Osman, R. M. (2024). Recent advances in transesterification for sustainable biodiesel production , challenges , and prospects : a comprehensive review. Environmental Science and Pollution Research, 31(9), 12722–12747. https://doi.org/10.1007/s11356-024-32027-4
37. Monika, Pathak, V. V., & Banga, S. (2026). A comprehensive analysis of refining technologies for biodiesel purification. Brazilian Journal of Chemical Engineering, 1–17.
38. Montgomery, D. C. (2017). Design and analysis of experiments (Ninth Edit). John Wiley & Sons.

39. Nair, A. T., Makwana, A. R., & Ahammed, M. M. (2018). The use of response surface methodology for modelling and analysis of water and wastewater treatment processes : a review. November, 464–478. https://doi.org/10.2166/wst.2013.733
40. Narasimharao, K., Mostafa, M. M. M., Al-amshany, Z. M., & Bajafar, W. (2023). Mechanochemical Synthesized CaO/ZnCo 2 O 4 Nanocomposites for Biodiesel Production. Catalysts, 13(2), 398.
41. Nawin, L., Kumar, M., & Thakur, C. (2024). Application of Catalysts Used in Biodiesel Production - A Review. Journal of Environmental Nanotechnology, 13(3), 145–151.
42. Odisu, T., Akemu, A., Obahiagbon, K. O. ., & Anih, E. C. (2019). Comparative Studies on the Production of Biodiesel from Shea Nut Oil by Acid Catalyzed and Supercritical Transesterification Processes. Appl. Sci. Environmental Management., 23(2), 349–357. https://doi.org/https://dx.doi.org/10.4314/jasem.v23i2.23
43. Okoduwa, I. G., Oiwoh, O., Amenaghawon, A. N., & Okieimen, C. O. (2025). A biobased mixed metal oxide catalyst for biodiesel production from waste cooking oil: reaction conditions modeling, optimization and sensitivity analysis study. Journal of Engineering Research (Kuwait), 13(2), 1344–1357. https://doi.org/10.1016/j.jer.2024.03.009
44. Olubunmi, B. E., Karmakar, B., Aderemi, O. M., G, A. U., Auta, M., & Halder, G. (2020). Journal of Environmental Chemical Engineering Parametric optimization by Taguchi L9 approach towards biodiesel production from restaurant waste oil using Fe-supported anthill catalyst. Journal of Environmental Chemical Engineering, 8(5), 104288. https://doi.org/10.1016/j.jece.2020.104288
45. Osorio-Tejada, J. L., Llera-Sastresa, E., & Scarpellini, S. (2017). A multi-criteria sustainability assessment for biodiesel and liquefied natural gas as alternative fuels in transport systems. Journal of Natural Gas Science and Engineering, 42, 169–186. https://doi.org/10.1016/j.jngse.2017.02.046
46. Patiño, Y., Faba, L., Peláez, R., Cueto, J., Marín, P., Díaz, E., & Ordóñez, S. (2023). The Role of Ion Exchange Resins for Solving Biorefinery Catalytic Processes Challenges. Catalysts, 13(6), 999.
47. Qader, D. N., Jamil, A. S., Bahrami, A., Ali, M., & Arunachalam, K. P. (2025). A systematic review of metakaolin-based alkali- activated and geopolymer concrete : A step toward green concrete. Reviews on Advanced Materials Science, 64(1), 20240076.
48. Qurashi, F., Sial, S. A., & Qureshi, H. H. (2026). Recent developments in biodiesel synthesis from agricultural wastes : A comprehensive review of feedstocks , catalysts , and machine learning approaches. SciNex Journal of Advanced Sciences., 1(01), 202510060007–202510060007. https://doi.org/10.sjas.202510060007
49. Ramesh, M., Praveen, S., Kuppuswamy, N., Khan, A., & Asiri, A. M. (2021). Biodiesel production from waste cooking oil using ionic liquids as catalyst. Advanced Technology for the Conversion of Waste into Fuels and Chemicals: Volume 1: Biological Processes, 91, 215–230. https://doi.org/10.1016/B978-0-12-823139-5.00005-8
50. Rezania, S., Sotoudehnia, Z., Ali, M., Cho, J., Kumar, K., Cabral-pinto, M. M. S., Alam, J., Ahamed, M., & Rashidi, H. (2021). Lanthanum phosphate foam as novel heterogeneous nanocatalyst for biodiesel production from waste cooking oil. Renewable Energy, 176, 228–236. https://doi.org/10.1016/j.renene.2021.05.060
51. Rizwanul Fattah, I. M., Ong, H. C., Mahlia, T. M. I., Mofijur, M., Silitonga, A. S., Ashrafur Rahman, S. M., & Ahmad, A. (2020). State of the Art of Catalysts for Biodiesel Production. Frontiers in Energy Research, 8, 101. https://doi.org/10.3389/fenrg.2020.00101
52. Satriadi, H., Setyojati, P. W., Shihab, D., Buchori, L., Hadiyanto, H., & Nurushofa, F. A. (2024). Preparation CaO / MgO / Fe 3 O 4 magnetite catalyst and catalytic test for biodiesel production. Results in Engineering, 22, 102202. https://doi.org/10.1016/j.rineng.2024.102202
53. Singh, D., Singh, K., Jadeja, Y., Menon, S. V, Singh, P., Ibrahim, S. M., & Singh, M. (2025). Magnetic nano-sized solid acid catalyst bearing sulfonic acid groups for biodiesel synthesis and oxidation of sulfides. Scientific Reports, 15, 1397. https://doi.org/https://doi.org/10.1038/s41598-024-84494-x
54. Sisca, V., Zilfa, Jamarun, N., & Tanjung, D. A. (2025). Catalytic innovation for renewable energy: TiO_2-supported precipitated calcium carbonate catalyst for biodiesel synthesis. Baghdad Science Journal, 22(3), 11692.
55. Sun, J., Chen, H., Shen, H., Luo, X., & Lin, Z. (2026). Optimization of Biodiesel Production from Waste Cooking Oil Using a Construction Industry Waste Cement as a Heterogeneous and Reusable Catalyst. 16(2), 108. https://doi.org/https://doi.org/10.3390/nano16020108

56. Suryanto, A., Kalsum, R. R. U., Munira, M., Syahrir, M., & Falah, N. N. I. A. (2025). Evaluation of Potassium Carbonate-Impregnated Alumina Catalyst In Batch Biodiesel Production From Castor Oil. International Journal on Technical and Physical Problems of Engineering (IJTPE), 17, 144–150.\
57. Suwanthai, W., Punsuvon, V., & Vaithanomsat, P. (2016). Optimization of biodiesel production from a calcium methoxide catalyst using a statistical model. Korean Journal of Chemical Engineering, 33(1), 90–98. https://doi.org/10.1007/s11814-015-0096-9
58. Tang, C. F., Tan, B. W., & Ozturk, I. (2016). Energy consumption and economic growth in Vietnam. Renewable and Sustainable Energy Reviews, 54, 1506–1514. https://doi.org/10.1016/j.rser.2015.10.083
59. Tien, T., Kee, M., Wang, Y., Loke, P., Shi, I., & Lim, S. (2021). Reaction kinetic and thermodynamics studies for in-situ transesterification of wet microalgae paste to biodiesel. Chemical Engineering Research and Design, 169, 250–264. https://doi.org/10.1016/j.cherd.2021.03.021
60. Turcu, E., Coromelci, C. G., Harabagiu, V., & Ignat, M. (2023). Enhancing the photocatalytic activity of TiO2 for the degradation of congo red dye by adjusting the ultrasonication regime applied in its synthesis procedure. Catalysts, 13(2), 345.
61. Ulukardesler, A. H. (2023). Biodiesel Production from Waste Cooking Oil Using Different Types of Catalysts. Processes, 11(7), 2035. https://doi.org/https://doi.org/10.3390/pr11072035
62. Vakhitova, Z. I., & Alston-Knox, C. L. (2018). Non-significant p-values? Strategies to understand and better determine the importance of effects and interactions in logistic regression. PLoS ONE, 13(11), e0205076. https://doi.org/10.1371/journal.pone.0205076
63. Wang, B., Wang, B., Shukla, S. K., & Wang, R. (2023). Enabling Catalysts for Biodiesel Production. Catalysts, 13(4), 740. https://doi.org/https://doi.org/10.3390/catal13040740
64. Yaghi, M., Chidiac, S., Awad, S., Rayess, Y. El, & Zgheib, N. (2025). An Overview of Biodiesel Production via Heterogeneous Catalysts : Synthesis , Current Advances , and Challenges. Clean Technologies, 7(3), 62. https://doi.org/10.3390/cleantechnol7030062
65. Yang, G., & Yu, J. (2023). Advancements in Basic Zeolites for Biodiesel Production via Transesterification. Chemistry, 5(1), 438–451. https://doi.org/10.3390/chemistry5010032
66. Yesilyurt, M. K., Cesur, C., Aslan, V., & Yilbasi, Z. (2020). The production of biodiesel from safflower (Carthamus tinctorius L.) oil as a potential feedstock and its usage in compression ignition engine: A comprehensive review. Renewable and Sustainable Energy Reviews, 119(109574). https://doi.org/10.1016/j.rser.2019.109574
67. Yusuff, A. S., Gbadamosi, A. O., & Popoola, L. T. (2021). Journal of Environmental Chemical Engineering Biodiesel production from transesterified waste cooking oil by zinc-modified anthill catalyst : Parametric optimization and biodiesel properties improvement. Journal of Environmental Chemical Engineering, 9(2), 104955. https://doi.org/10.1016/j.jece.2020.104955
68. Zaera, F. (2022). Designing Sites in Heterogeneous Catalysis : Are We Reaching Selectivities Competitive With Those of Homogeneous Catalysts ? Chemical Reviews, 122(9), 8594–8757. https://doi.org/10.1021/acs.chemrev.1c00905
69. Zaman, K., & Moemen, M. A. el. (2017). Energy consumption, carbon dioxide emissions and economic development: Evaluating alternative and plausible environmental hypothesis for sustainable growth. Renewable and Sustainable Energy Reviews, 74, 1119–1130. https://doi.org/10.1016/j.rser.2017.02.072
70. Zhang, Y., Niu, S., Han, K., Li, Y., & Lu, C. (2021). Synthesis of the SrO–CaO–Al2O3 trimetallic oxide catalyst for transesterification to produce biodiesel. Renewable Energy, 168, 981–990. https://doi.org/10.1016/j.renene.2020.12.132
71. Zhang, Y., Li, X., Wang, H., & Chen, Y. (2025). Enhanced anti-sintering performance of metakaolin incorporated CaO adsorbents for CO_2 capture. Journal of Environmental Chemical Engineering, 13, 118734. https://doi.org/10.1016/j.jece.2025.118734